Comparative analysis of the syncytiotrophoblast in placenta tissue and trophoblast organoids using snRNA sequencing

Madeline M Keenen[1], Liheng Yang[2], Huan Liang[1,3], Veronica J Farmer[1], Rohit Singh[1,3], Amy S Gladfelter[1]*, and Carolyn B Coyne[2,4]*

1) Duke University School of Medicine, Department of Cell Biology, Durham, NC
2) Duke University School of Medicine, Department of Integrative Immunobiology, Durham, NC
3) Duke University School of Medicine, Department of Biostatistics and Bioinformatics
4) Duke Human Vaccine Institute, Durham, NC

*Address correspondence:

Carolyn Coyne, PhD
3130 Medical Sciences Research Building III
3 Genome Court
Durham, NC 27710
USA
carolyn.coyne@duke.edu

Amy Gladfelter, PhD
C341 LSRC
308 Research Drive
Durham, NC 27708
amy.gladfelter@duke.edu

Abstract

The outer surface of chorionic villi in the human placenta consists of a single multinucleated cell called the syncytiotrophoblast (STB). The unique cellular ultrastructure of the STB presents challenges in deciphering its gene expression signature at the single-cell level, as the STB contains billions of nuclei in a single cell. There are many gaps in understanding the molecular mechanisms and developmental trajectories involved in STB formation and differentiation. To identify the underlying control of the STB, we performed comparative single nucleus (SN) and single cell (SC) RNA sequencing on placental tissue and tissue-derived trophoblast organoids (TOs). We found that SN was essential to capture the STB population from both tissue and TOs. Differential gene expression and pseudotime analysis of TO-derived STB identified three distinct nuclear subtypes reminiscent of those recently identified *in vivo*. These included a juvenile nuclear population that exhibited both CTB and STB marker expression, a population enriched in genes involved in oxygen sensing, and a fully differentiated subtype. Notably, suspension culture conditions of TOs that restore the native orientation of the STB (STB^{out}) showed elevated expression of canonical STB markers and pregnancy hormones, along with a greater proportion of the terminally differentiated mature STB subtype, compared to those cultivated with an inverted STB polarity (STB^{in}). Gene regulatory analysis identified novel markers of STB differentiation conserved in tissue and TOs, including the chromatin remodeler RYBP, that exhibited STB-specific RNA and protein expression. Finally, we compared STB gene expression signatures amongst first trimester tissue, full-term tissue, and TOs, identifying many commonalities but also notable variability across each sample type. This indicates that STB gene expression is responsive to its environmental context. Our findings emphasize the utility of TOs to accurately model STB differentiation and the distinct nuclear subtypes observed *in vivo*, offering a versatile platform for unraveling the molecular mechanisms governing STB functions in placental biology and disease.

Introduction

During the course of human gestation, the developing fetus forms an entire organ to support its growth—the placenta. While the fetal organs undergo development, the placenta assumes a multifaceted role, serving to facilitate molecular exchange, perform essential metabolic functions, produce hormones, prevent loss of immune tolerance, and act as a barrier against the vertical transmission of pathogens (Aye et al., 2022; Benirschke et al., 2012; Costa, 2016; Megli and Coyne, 2021). The placenta's remarkable complexity is underscored by its distinctive cellular architecture. Its outer layer encompasses a giant single cell called the syncytiotrophoblast (STB), that contains billions of nuclei and envelops the chorionic villi (Barker et al., 1973; Burton and Jauniaux, 1995; Haeussner et al., 2014). The STB is formed via cell-cell fusion of the underlying cytotrophoblast (CTB) cell population. CTBs reside on the basement membrane of chorionic villi to contribute new nuclei into the STB or lie at the interface between the placenta villi and the maternal decidua in multi-cell layered structures termed cell columns (CTB-CC) (**Figure 1A**) (Boyd and Hamilton, 1970). CTBs closer to the maternal decidua are more differentiated than their counterparts lower in the column, and eventually undergo epithelial to mesenchymal transition (EMT) to form fully differentiated extravillous trophoblast cells (EVT) that invade into the decidua (**Figure 1A**) (Arutyunyan et al., 2023; Turco and Moffett, 2019). The molecular mechanisms and environmental cues that drive CTB differentiation into either STB or EVT lineages is an area of active research and defining these trajectories are essential to understand placenta development and pathogenesis.

Several groups have applied single-cell RNA sequencing (SC) of primary tissue throughout gestation, trophoblast organoids (TOs), and trophoblast stem cells (TSCs) to characterize EVT differentiation (Arutyunyan et al., 2023; Li et al., 2024; Liu et al., 2018; Marsh et al., 2022; Pique-Regi et al., 2019; Shannon et al., 2024; Suryawanshi et al., 2018; Vento-Tormo et al., 2018). This has generated a lineage map of EVT differentiation with identification of its terminal states and the potential transcription factors involved. However, these datasets lack gene expression information from the STB due to technical challenges processing a giant, multinucleated cell. Therefore, approaches like single nucleus RNA sequencing (SN) may be essential to properly capture the heterogeneity of STB gene expression. In fact, a recent study performed SN on placenta tissue (six first trimester and six full-term tissues) and captured STB nuclei and defined their lineage trajectories at each gestational age (Wang et al., 2024). This study revealed the STB can bifurcate into two nuclear lineages post-fusion, associated with either hormone expression and GTPase signaling or with an oxygen response. This suggests different functions of the STB may be attributed to distinct individual nuclei within the same giant cell. However, how nuclei

with distinct gene expression arise and how they impact the function of the entire STB cell is not known. Dissecting nuclear heterogeneity in the STB will require a molecular biology and genetic toolkit that has been largely inaccessible for human pregnancy models.

A major challenge in establishing genetically tractable and accessible models for the human placenta is the remarkable diversity of placental structures amongst mammals, and notably the variations in the tissue architecture and cell types seen even between humans and mice (Hemberger et al., 2020; Wooding and Burton, 2008). In the last several years, trophoblast organoids (TOs) have emerged as powerful tools for studying trophoblast differentiation. CTB progenitor cells can be isolated from tissue throughout gestation, as CTB remain mitotic throughout pregnancy (Haider et al., 2018; Mayhew, 2014; Turco et al., 2019; Yang et al., 2022). They can subsequently be maintained in a proliferative state capable of trophoblast differentiation by using a growth factor cocktail and cultivation in extracellular matrix (Okae et al., 2018; Turco et al., 2019; Yang et al., 2022), and spontaneously fuse to form STB (Haider et al., 2018; Li et al., 2023; Turco et al., 2019; Yang et al., 2022). In standard culture conditions, TOs exhibit an inverted architecture compared to placental villi *in vivo*, with an outward facing proliferative CTB layer and a largely inward facing STB (STB^{in}) (Haider et al., 2018; Turco et al., 2019; Yang et al., 2022). Our recent work has established a method to reverse the cellular polarity of TOs to their native orientation, resulting in organoids containing very large (>50 nuclei) STB on the outermost layer and mononuclear CTBs positioned in the center (STB^{out}), and exhibit increased secretion of the STB-associated hormone human chorionic gonadotropin (hCG) (Yang et al., 2023). While the majority of CTBs differentiate into the STB in TOs, a small proportion can spontaneously differentiate into HLA-G^+ EVTs. This EVT percentage can be increased through a three-step treatment involving Neuregulin-1 (NRG1) (EVT^{enrich}) (Haider et al., 2018; Turco et al., 2019; Yang et al., 2022). Consequently, TOs offer the ability to induce differentiation along both STB and EVT lineages and have rapidly become a powerful and accessible tool to investigate trophoblast biology.

As TOs become increasingly prevalent as a research model, it is crucial to assess their resemblance to *in vivo* trophoblast cell types. In particular, the gene expression signature of the STB and any heterogeneity that exists amongst nuclei remains enigmatic due to its unique ultrastructure, both i*n vitro* and *in vivo*. In this study, we performed comparative SC and SN on primary full-term placenta tissue and TOs. We found that SN is essential to capture STB gene expression both in tissue and TOs, while SC enriches for maternal immune cells and the EVT lineage in tissue. Differential gene expression and pseudotime analysis of distinct STB in TOs

identified three distinct subtypes reminiscent of those recently identified *in vivo*: a juvenile population that exhibits both CTB and STB expression, an FLT1 expressing population enriched in genes involved in oxygen sensing, and a fully differentiated subtype enriched in expression of transport and GTPase signaling molecules. While STB^{in} and STB^{out} conditions maintain a similar proportion of mitotic cell nuclei, STB^{out} organoids exhibited a higher proportion of terminally differentiated STB nuclei and increased expression of STB-specific hormones. Both pseudotime and gene regulatory network analysis of RNA velocity identified genes linked to STB differentiation, including the chromatin effector RYBP, which is enriched in STB^{out} TOs. Finally, STB gene expression was compared between TOs and primary tissue at different stages of gestation. While CTBs were remarkably similar across all conditions, the STB displayed both commonalities and notable variability across the sample types. Together, this work demonstrates the capacity of TOs to mirror STB differentiation and the nuclear subtypes seen in *in vivo*, providing an accessible platform to dissect the key molecular pathways underlying placenta function, distinct STB subtypes, and trophoblast-related pregnancy disorders.

Results

Single nucleus sequencing is necessary to capture the gene expression signature of STBs in placental tissue and TOs

In this study, we set out to compare the transcriptional profile of full-term placental tissue composed of placental villi and decidua (**Figure 1A, 1B**) to STB^{in} TOs previously derived from placental tissue (**Figure 1B**). To assess whether SC or SN sequencing could effectively capture trophoblast cell populations, we processed matched samples into single cells/syncytial fragments or single nuclei (**Figure 1C, Materials and Methods**). The SC and SN datasets generated from primary placental tissue (**Figure 1 D-F**) and TOs (**Figure 1 G-I**) were integrated, and a graph-based clustering approach used to identify clusters (Butler et al., 2018; Hao et al., 2021; Satija et al., 2015; Stuart et al., 2019). Each dataset was visualized with a UMAP plot (**Figure 1D** and **1G**) and established gene expression markers were used to determine the cell or nuclear identity of each cluster (**Figure 1F**, **1I**, **Supplementary Figure 1.1C and 1.1F, and Supplemental Table 1-2**) (Arutyunyan et al., 2023; Derisoud et al., 2024; Vento-Tormo et al., 2018).

To determine how each sequencing technique affects the detection of trophoblast cell types, we first defined the cell/nucleus types in the primary tissue dataset. We identified two CTB subtypes, seven STB subtypes, and two EVT subtypes, each expressing their respective markers (e.g., PAGE4, CYP19A1, and HLA-G) (**Figure 1D, 1F, Supplemental Figure 1.1C**). There was a similar distribution of these subtypes across all three donor tissues (**Supplemental Figure 1.1A-B**). As in previous single cell approaches, our SC tissue dataset captured only a small fraction of the STB cell type (6% of total cells are STB). In contrast, the predominant population in the SN preparation was STB nuclei, accounting for 76% of the total nuclei count, (**Figure 1D-1E** and **Supplemental Figure 1.1A-B**) and consistent with their relative prevalence *in vivo* (Mayhew, 2014; Mayhew and Simpson, 1994; Simpson et al., 1992). Of note, the SN dataset on primary tissue had an 8:1 ratio of STB to CTB, resembling stereological estimates of placental trophoblast compositions at full-term (9:1) indicating that enzymatic digestion of nuclei is capturing a near representative population of these trophoblast nucleus types. (**Figure 1D**). While the STB subtype is better captured by SN sequencing, SC sequencing exhibited significant enrichment in both EVT (18% of total in SC vs. 1.3% in SN) and macrophages (53% of total in SC vs. 1.9% in SN) (**Figure 1D-1E** and **Supplemental Figure 1.1A-B)**. As a control for SC/SN dataset integration, cell/nucleus types were identified within the individual SC and SN datasets and proportions mirrored the integrated SC/SN

dataset (**Supplemental Figure 1.2 and 1.3**). This demonstrates that differences between tissue processing for either SC or SN impact the cell types recovered and subsequently sequenced.

We next defined the nucleus types represented in the STB^{in} TO dataset, in which we identified two proliferating CTB populations (CTB-p), five non-proliferative CTB clusters (CTB-1-5), one pre-fusion CTB population with high expression of endogenous retroviral fusion genes (CTB-pf), and two STB populations (STB 1-2) (**Figure 1G-1I** and **Supplemental Figure 1.1F**). Like placental tissue, the SC dataset captured only a small number of the total STB present in TOs, with only 2.4% of the total cell population attributed to the STB (**Figure 1G** and **Supplemental Figure 1.1E**). In contrast, the STB accounted for 38% of the total nucleuar numbers captured by SN sequencing (**Figure 1G** and **Supplemental Figure 1.1E**). The differences in non-proliferative CTB populations (CTB 1-5) between SC and SN sequencing were less pronounced, with 57% of the total cell population from SC sequencing attributed to these cells and 56% of nuclei in the SN dataset (**Figure 1G** and **Supplemental Figure 1.1E**). Similarly, both SC and SN captured nearly identical numbers of CTB-pf cells (7%). However, the number of CTB-p were only 16% of the total population in SN despite accounting for 40% in SC, consistent with the challenge to isolate nuclei from mitotic cells for SN sequencing due to the breakdown of the nuclear envelope during mitosis (**Figure 1G**). Collectively, this comparison underscores the necessity of SN sequencing to representatively capture the gene expression of the STB population in both primary placental tissue and TOs.

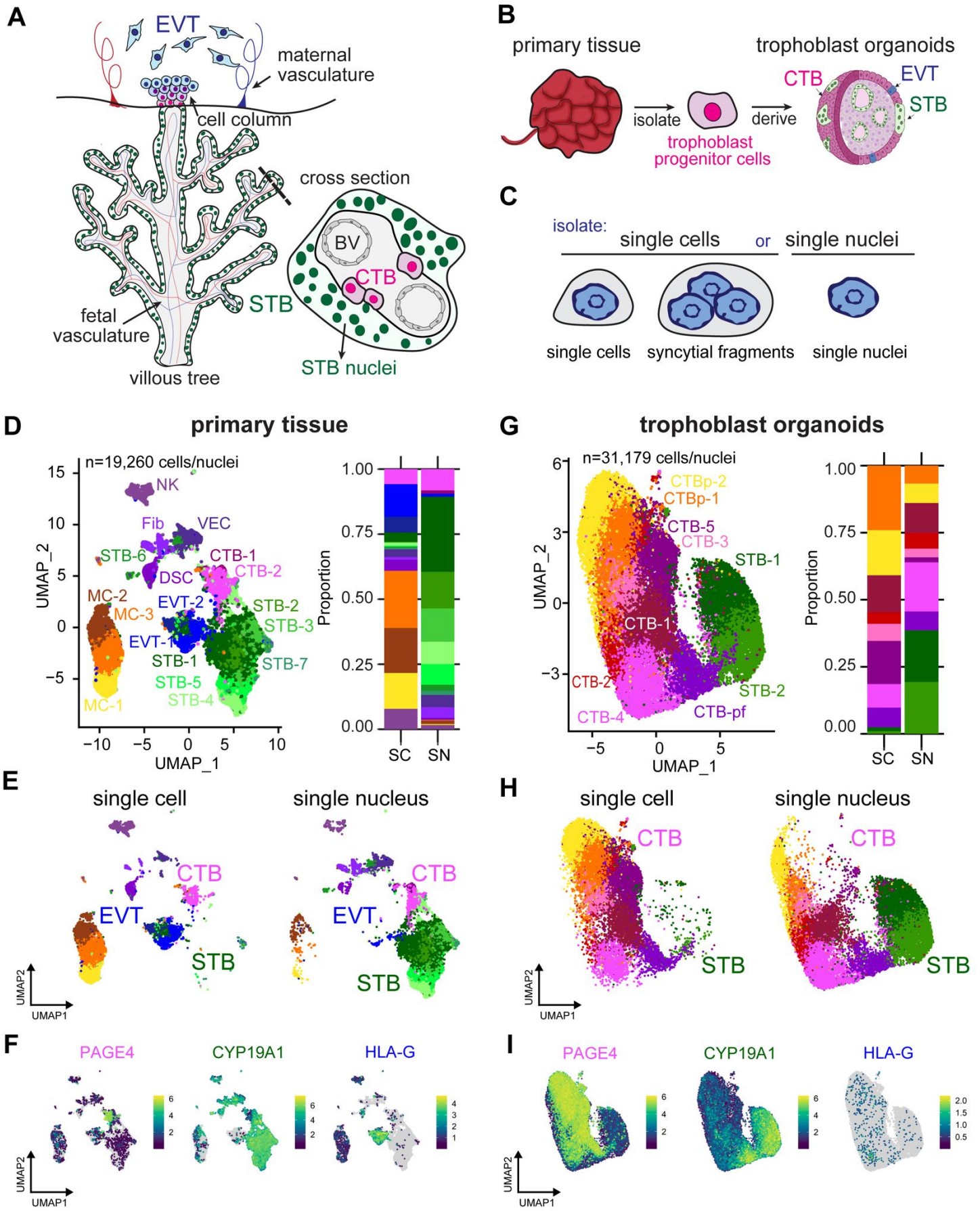

Figure 1: Single nucleus sequencing is essential to capture the STB lineage in full-term tissue and TOs. **A** Cartoon of placenta villous tree and cross section, with the multinucleated STB highlighted in green, progenitor

CTB cells in magenta, and extravillous cytotrophoblasts in blue. **B** Schematic of organoid generation via isolation of trophoblast progenitor cells from full-term placental tissue. **C** Schematic of experimental setup. Both tissue and TOs were processed into either single cells/syncytial fragments or single nuclei and sequenced. UMAP of integrated SC and SN datasets collected from primary tissue (**D**) and TOs (**G**). Cell/nucleus types are annotated as follows: cytotrophoblast (CTB), cytotrophoblast pre-fusion (CTB-pf), syncytiotrophoblast (STB), extravillous trophoblast (EVT), dendritic stem cell (DSC), vascular endothelial cell (VEC), fibroblasts (Fib), natural killer cell (NK), and macrophage (MC). Cell/nucleus types that contained multiple clusters are identified with -number after the name. **E and H** UMAP of the integrated SC and SN dataset separated into individual UMAPs by single cell or nucleus processing type for primary tissue (E) and TOs (H). **F and I** Expression of key trophoblast markers, including PAGE4 (CTB), CYP19A1 (STB), and HLA-G (EVT) in primary tissue (F) and TOs (I).

Defining trophoblast lineage composition in distinct TO culture conditions

We next investigated the impact of TO culture conditions on trophoblast lineage composition using SN sequencing because it more accurately captured the STB population. To do this, we used TOs isolated from three unique placentas and cultured them each in three distinct culture conditions—standard Matrigel conditions to generate STB^{in} TOs, in suspension to generate STB^{out} TOs, and with NRG1 to enrich for EVT cells (EVT^{enrich}) (**Figure 2A-C, Materials and Methods, Supplemental Table 3-4**). Each organoid condition was processed into suspensions of nuclei, SN sequenced in parallel, and data from each biological replicate integrated, clustered, and plotted on a UMAP (**Figure 2A-C, Supplementary Figure 2.1A, Supplemental Table 1-2)**.

We first assessed how CTB subtypes varied amongst the culturing methods that generated different organoid organizations. We found five populations of CTBs that were identified using well-established markers, such as CDH1 and TENM3, and accounted for 53% of the total population in STB^{in}, 38% in STB^{out}, and 57% in EVT^{enrich} (**Figure 2A-C, Supplementary Figure 2.1B**). These CTBs could be delineated into multiple subtypes expressing proliferative markers (KI67 and PCNA in CTB-p), CTB cell column (CTB-CC) markers (LPCAT1, NOTCH1, and ITGA2), or pre-fusion intermediate markers (retroviral fusion protein ERVFRD-1 and GREM2 in CTB-pf) (**Supplementary Figure 2.1B**). STB^{in} and STB^{out} TOs both contained two proliferative CTB populations (CTBp-1 and CTBp-2) that together accounted for 18% of the total nuclear population of each dataset (**Figure 2A-B**). In contrast, there was a single proliferative population in EVT^{enrich} that accounted for 10% of the population, was closer to EVT than CTB on the UMAP, and had downregulated CTB markers and upregulated EVT markers including HLA-G and MMP2. This suggests that TO-derived differentiated EVTs undergo mitosis, as observed *in vivo* (**Figure 2C, Supplementary Figure 2.1B, D**) (Arutyunyan et al., 2023). In the STB^{in} condition, CTB-2 expressed canonical CTB-CC markers and accounted for 17% of the total nuclear population (**Supplementary Figure 2.1B-C**). The STB^{out} condition predominantly consisted of a single non-proliferative CTB population (CTB-1). A subset of this cluster expressed the CTB-CC marker ITGA2 suggesting this CC population was still present

but not identified as a separate cluster (**Supplementary Figure 2.1B-C**). In contrast, three of the five CTB populations in EVT^{enrich} TOs expressed the CTB-CC markers ITGB6 and LPCAT1 (**Supplementary Figure 2.1B-C**), consistent with the function of CTB-CCs to differentiate into EVT (Turco and Moffett, 2019). Finally, CTB-pf accounted for 4% of the total population in STB^{out}/EVT^{enrich} TOs and 6% of STB^{in}, suggesting culture conditions did not dramatically change the proportion of this intermediate cell type (**Figure 2A-C, Supplementary Figure 2.1B**). Thus, while most CTB identities are present across conditions, there are notable differences in the proportion of different trophoblast types depending on culture conditions.

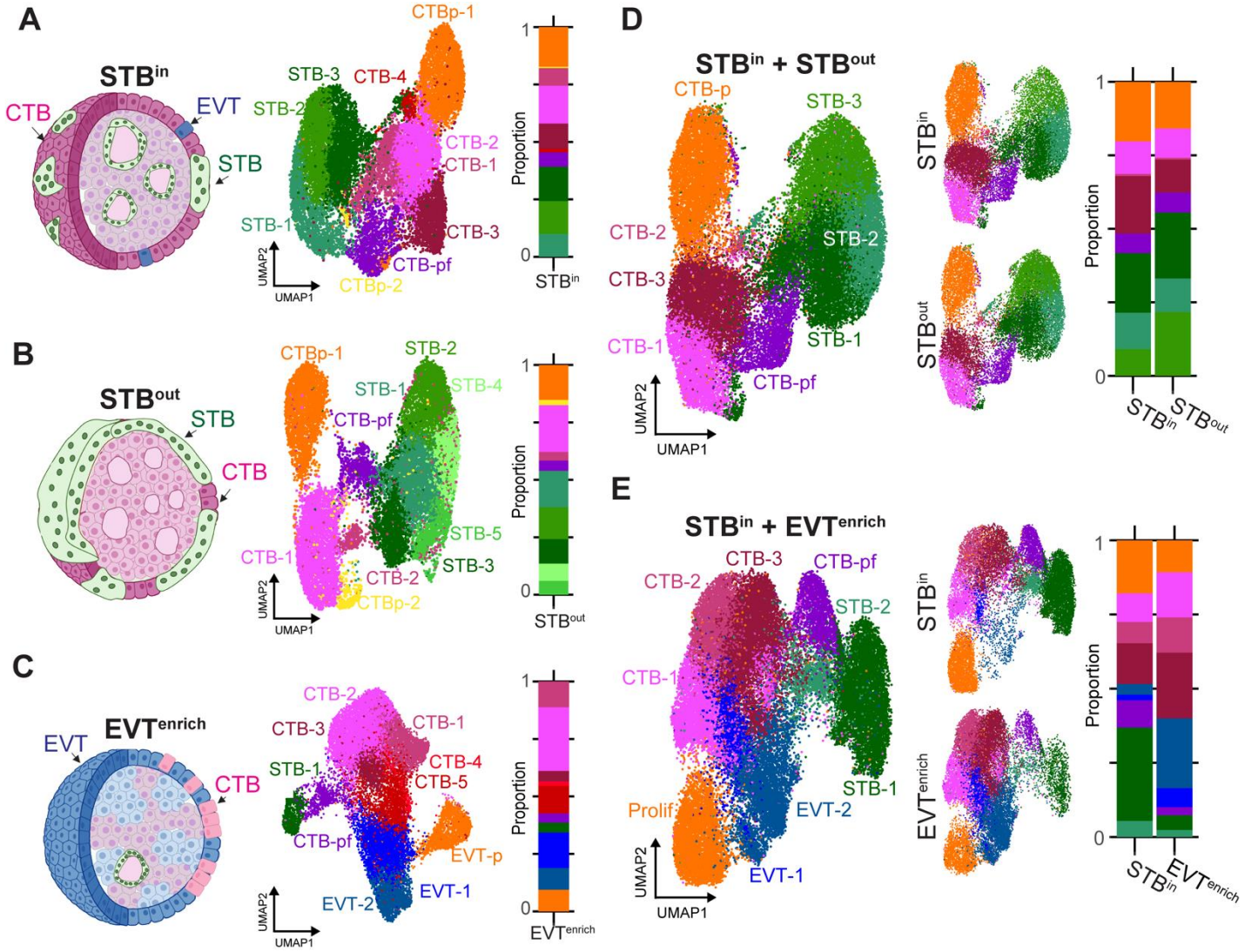

Figure 2: Comparison of TO gene expression in different culture conditions by SN RNA sequencing. TOs were grown with the STB facing inward (STB^{in}), outward (STB^{out}), or induced to differentiate into EVT (EVT^{enrich}). Schematic of TO nucleus type composition (left), UMAP of the individual SN datasets (middle), and barplot showing the proportions of each nucleus type (right) are shown for STB^{in} (**A**), STB^{out} (**B**), or EVT^{enrich} (**C**). UMAP of the integrated datasets (left), integrated dataset split by culture condition (middle), and barplot showing the proportions of each nucleus type (right) are shown for the STB^{in}+STB^{out} integrated dataset (**D**) or STB^{in}+EVT^{enrich} dataset (**E**).

We next sought to determine how culture conditions influenced the differentiation of CTBs into either the STB or EVTs. In each culture condition STB nuclei were present, accounting for 39% (STB^{in}), 53% (STB^{out}), and 4% (EVT^{enrich}) of the total population (**Figure 2A-C**). As anticipated, few to no EVTs were present in STB^{in} and STB^{out} TOs (**Figure 2A-B)** (Turco et al., 2019; Yang et al., 2023, 2022). In contrast, EVTs accounted for 24% of the total population in EVT^{enrich} TOs and separated into two clusters (EVT-1, EVT-2) (**Figure 2C**). Each had an increased expression of the mature EVT markers HLA-G, MMP2, and DIO2 (**Supplemental Figure 2.1B**). Together, this demonstrates that STB^{out} culture conditions promotes further STB differentiation while EVT^{enrich} conditions promotes EVT differentiation.

To directly compare the relative populations and gene expression between TO culture conditions, we integrated the STB^{in} dataset with either STB^{out} or EVT^{enrich} TOs (**Figure 2D-E**). Each nucleus type retained the expression of canonical markers (**Supplemental Figure 2.2A-B**), but EVT^{enrich} exhibited higher basal expression of the EVT markers HLA-G and DIO2 (**Supplemental Figure 2.2C**). The nucleus types in the STB^{in}+STB^{out} dataset showed significant overlap on the UMAP, indicating relatively consistent gene expression across culture conditions (**Figure 2D**). However, the proportions were not identical for each nucleus type and reflected the differences observed in the individual datasets. Of note, there was a higher percentage of CTB-3 that expressed CTB-CC markers in STB^{in} (20% of STB^{in} and 11% of STB^{out}) and a decrease in the STB-3 population (9% of STB^{in} and 20% of STB^{out}) (**Figure 2D, Supplemental Figure 2.2A**) suggesting that STB^{out} culture conditions promotes STB differentiation and prevents CTB-CC differentiation down the EVT lineage. Despite CTB-pf accounting for 7% of each dataset in STB^{in} and STB^{out}, the STB:CTB ratio was nearly halved in STB^{in} compared to STB^{out} (1.3:1 in STB^{in} versus 2.5:1 in STB^{out}). This indicates a higher proportion of nuclei in STB^{out} TOs have moved into the STB (**Figure 2B**). Similarly, STB^{out} TOs expressed higher levels of key STB markers and hormones, indicating culture in suspension promotes enhanced STB differentiation (**Supplementary Figure 2.2D and Supplementary Figure 3.1D**). These results are consistent with our previous report demonstrating an increase in the number of STB nuclei and enhanced expression of hCG- genes in the STB^{out} condition (Yang et al., 2023). In contrast, the STB^{in}+EVT^{enrich} merged dataset exhibited significantly less overlap on the UMAP and amongst nucleus type proportions (**Figure 2E**). In particular, STB^{in} TOs had a dramatic increase in STB nucleus types (37% of STB^{in} and 7% of EVT^{enrich}) while EVT^{enrich} exhibited an increase in EVT types (5% of STB^{in} and

30% of EVT^{enrich}) (**Figure 2E, Supplemental Figure 2.2B**), validating EVT^{enrich} conditions promote CTB differentiation into EVT instead of STB.

Lastly, we compared STB^{out} TOs with a publicly available SN dataset from trophoblast stem cell (TSC) derived STB to identify differences in STB populations that might exist between these models (Wang et al., 2024). We integrated the STB^{out} TO dataset with the TSC dataset, performed clustering, and visualized the results on a UMAP. Both TO and TSC models showed a nearly equivalent composition of trophoblast nucleus types, including CTB-p, CTB-pf, EVTs, and two distinct STB populations (STB-1 and STB-2) (**Supplemental Figure 2.3A-C**). Despite similarities in nuclear proportions, pseudobulk differential expression analyses revealed significant differences in the transcriptional profiles of CTB-pf and STB populations derived from TOs and TSCs. TSC-derived CTB-pf and STB clusters highly expressed the EVT marker HLA-G, which was absent in TO-derived CTB-pf and STBs (**Supplemental Figure 2.3D**). Additionally, TO-derived CTB-pf and STBs showed significantly higher expression of STB-associated hormones and other factors, including PSGs, CGBs, CSH1, HOPX, and KISS1 (**Supplemental Figure 2.3D-E**) (Costa, 2016). Therefore, while the two models exhibit a similar proportion of nucleus types, there are notable gene expression differences within each.

Together, these data highlight that culture conditions not only influence the composition of trophoblast nucleus types but also drive their differentiation into distinct lineages, consistent with previous reports and underscoring the critical role of the environmental cues present in each culture condition in shaping trophoblast identity (Arutyunyan et al., 2023; Turco and Moffett, 2019; Yang et al., 2023, 2022).

Comparative transcriptional profiling of STB nucleus subtypes between STB^{in} and STB^{out} TOs

Given the increased proportion of STB nuclei in STB^{out} TOs and enhanced expression of typical STB markers in STB^{out} TOs, we next sought to identify the genes that define each STB subtype. To do this, we utilized the merged STB^{in}+STB^{out} dataset that contained three STB subpopulations. This dataset exhibited differential enrichment of each STB subpopulation within the two culture conditions (**Figure 3A**). We first analyzed the genes enriched in each STB subtype and identified hundreds of genes whose expression was conserved in the STB subtypes of both STB^{in} and STB^{out} TOs (**Figure 3B, Supplemental Figure 3.1A**). STB-1 is closest to CTB-pf on the UMAP and expressed many genes previously associated with CTBs, including the transcription factors TEAD1 and TP63 (**Figure 2D, 3B, and 3D**) (Li et al., 2014; Mizutani et al., 2022). In fact, when the top genes in

STB-1 were plotted as a dotplot for every nucleus type in the dataset these genes were most enriched in the CTB subtypes (**Supplemental Figure 3.1B**). The gene ontology (GO) terms associated with STB-1-enriched genes are involved in RNA splicing, stem cell maintenance, and RAS signaling (**Figure 3C**). Candidate genes from each of these GO terms demonstrated expression predominantly in CTBs, intermediate expression in STB-1, and lower expression in the remaining two STB populations (**Figure 3D**). STB-2 expressed a unique subset of genes that included the VEGF receptor FLT1, the TGFβ family member INHBA, and the insulin regulator PAPPA2, associating this subtype with ER stress and oxygen sensing (**Figure 3B-C**) (Barrios et al., 2021; Li et al., 2022; Sasagawa et al., 2021, 2018). While female pregnancy was identified as an enriched GO term in STB-2, only a subset of pregnancy hormones was identified (**Figure 3C-D**). In fact, most pregnancy hormones were expressed at similar levels in the STB-2 and STB-3 subtypes (**Supplemental Figure 3.1C**). Both STB-1 and STB-2 were more abundant in STB^{in} than STB^{out} (**Figure 3A**). Finally, the top genes in STB-3 included the sodium/bicarbonate transporter SLC4A4, the matrix metalloprotease ADAMTS6, the collagen receptor ITGA1, and protein kinase C epsilon PRKCE (**Figure 3B**) (Cain et al., 2022, 2016; Zeltz and Gullberg, 2016). GO terms demonstrated that the STB-3 cluster was enriched for processes involved in GTPase signaling, vascular transport, and actin organization (**Figure 3C-D**). In contrast to STB-1 and STB-2, the percentage of STB-3 nuclei were doubled from 20% in STB^{in} to 40% in STB^{out}. Interestingly, most STB pregnancy hormones were more enriched in STB^{out} compared to STB^{in} and expressed in both STB-2 and STB-3 subtypes (**Supplemental Figure 3.1C-D**). In summary, STB-1 exhibited intermediate gene expression between CTB and STB, STB-2 expressed vascular signaling/oxygen sensing factors, while STB-3 was enriched in transport/GTPase signaling functions.

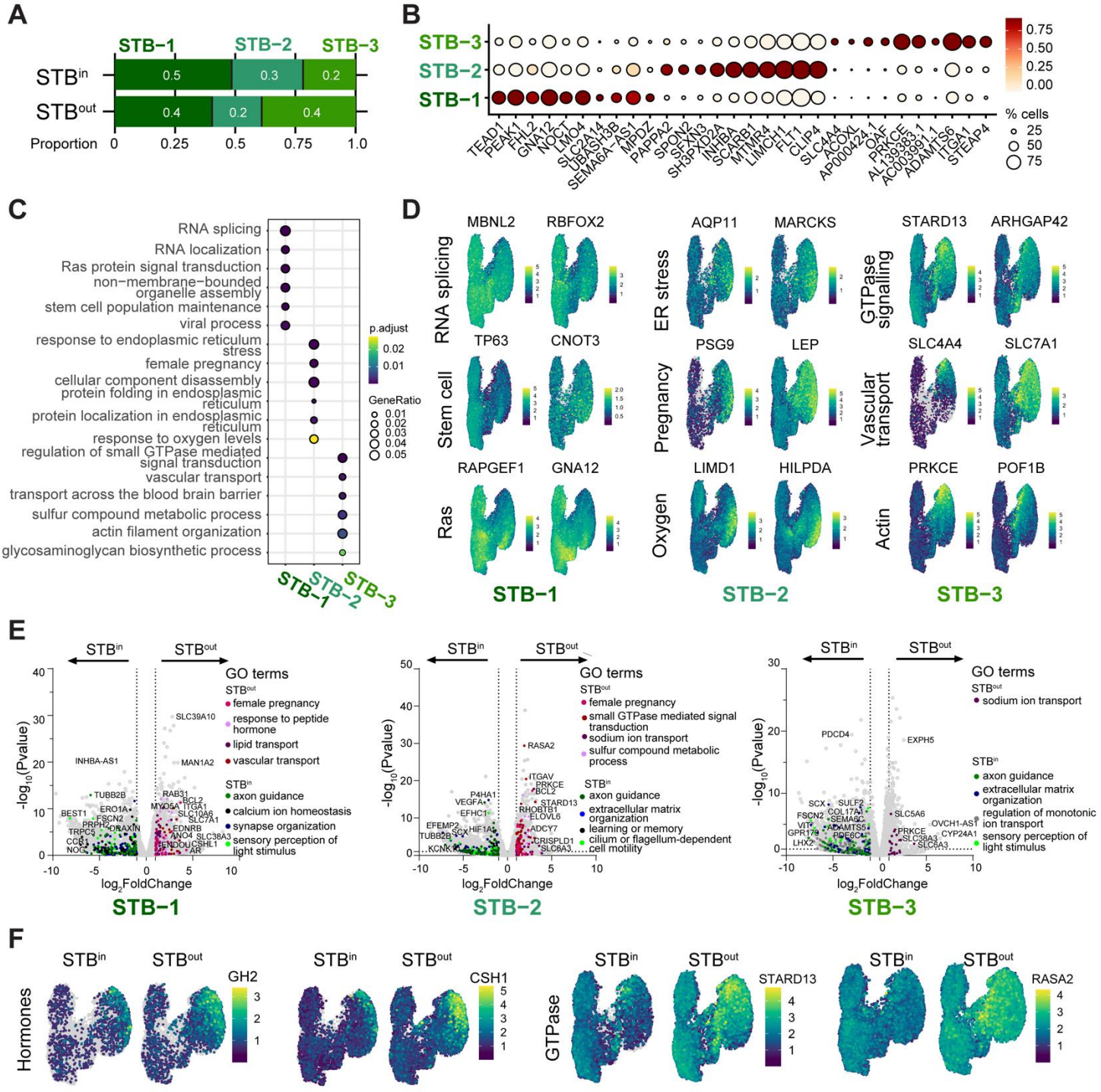

Figure 3: STB subtype analysis and expression differences in STB^{in} vs STB^{out} TOs. A Proportion of each STB subtype in the integrated STB^{in}+STB^{out} dataset. **B** Top differentially expressed genes (DEGs) of each STB subtype is shown as a dot plot. Mean expression is shown as a color scale and percent of nuclei expressing each gene is demonstrated by size of the dot. **C** Top Biological Process GO terms associated with DEGs in each STB subtype was determined with clusterProfiler. **D** Feature plots demonstrating RNA expression of candidate target genes from GO terms in C. **E** DEseq2 was used to find DEGs between STB^{in} and STB^{out} datasets in STB-1, STB-2, and STB-3 clusters and plotted as a volcano plot. GO terms associated with DEGs in either STB^{in} or STB^{out} were found with clusterProfiler and colored on the UMAP with select representative genes highlighted with text. **F** Feature Plot of representative target genes from E.

Given the different proportions of STB subtypes between STB^{in} and STB^{out} TOs, we next sought to determine if gene expression changed within each STB subtype as a function of culture condition. Therefore, we performed pseudobulk differential expression analysis using DESeq2 to compare gene expression of each STB subtype between STB^{in} and STB^{out} TOs and determined GO terms associated with the differentially expressed genes (DEGs) (**Figure 3E**) (Love et al., 2014). STB-1 and -2 of STB^{out} TOs were enriched for genes involved in pregnancy including genes in the human placenta lactogen family (CSH1 and CSHL1), growth hormone 2 (GH2), the STB specific gene ENDOU (Haider et al., 2018), and the androgen receptor (AR) (**Figure 3E-F**). In addition, STB in STB^{out} TOs exhibited increased expression of genes involved in GTPase signaling, including the RhoA GAPs STARD13 and GRAF3 (ARHGAP42) (Bai et al., 2013; Ching et al., 2003) (**Figure 3E-F**). All three STB subtypes in STB^{out} TOs exhibited an enrichment in transport-associated proteins, consistent with the STB being proximal to media (**Figure 3E, Supplemental Figure 3.1E**). In contrast, STB^{in} TOs were enriched in extracellular matrix organization genes but their expression was not specific to STB subtypes (**Figure 3E and Supplementary Figure 3.1F**). The STB-2 subtype in STB^{in} TOs had increased expression of the hypoxia associated genes LIMD1, HILPDA, and HIF1A as well as the angiogenesis-associated proteins VEGFA and FLT1 (**Figure 3E, Supplemental Figure 3.1G**) (Foxler et al., 2018; Rodriguez and Kersten, 2020; Shibuya, 2011), consistent with the increased proportion of the oxygen sensing STB-2 subtype in STB^{in}. Together, these results demonstrate that there are at least three subpopulations of STB in trophoblast organoids, which differ in their relative proportions and transcriptional signature between culture conditions.

Pseudotime and Velocity analysis reveals the enrichment of STB lineage markers and gene regulators in STB^{out} TOs

To assess whether distinct nucleus subtypes represented a STB differentiation trajectory in TOs, we next performed pseudotime gene expression inference using the integrated STB^{in} and STB^{out} datasets described above (**Figure 2D**). We utilized the Slingshot algorithm to establish the global lineage structure for each dataset using undefined starting and ending clusters (Street et al., 2018). Following this, we depicted the pseudotime progression on the UMAP plot for the STB lineage (**Figure 4A**). This visualization revealed a continuous trajectory starting from CTB-p subtype, traversing through CTBs to CTB-pf, and progressing through STB-1 and STB-2 before culminating in a terminally differentiated STB-3 subtype (**Figure 4A**). We found that STB

differentiation was marked by an increase in well-known STB marker genes, including ADAM12, PLAC4, and PSG6 (**Figure 4B**) (Aghababaei et al., 2015; Chen et al., 2022; Moore et al., 2021; Tuohey et al., 2013). Next, we conducted a comparative pseudotime expression analysis using tradeSeq between STB^{in} and STB^{out} conditions. Our findings revealed enrichment of several STB-associated genes in STB^{out}, such as the secreted metallopeptidase protein ADAM12, the progesterone synthesis enzyme CYP11A1, and the proteoglycan synthesis gene MAN1A2 (**Figure 4C**) (Aghababaei et al., 2015; Zhu et al., 2023). Given the STB-3 population is enriched in STB^{out} (**Figure 3A**) and represents the terminal differentiated state in the trajectory with pseudotime (**Figure 4A**), this supports the hypothesis that STB nuclei in the STB^{out} model are further differentiated than those in STB^{in}. This is consistent with the increased expression of STB differentiation markers and hormones in the STB^{out} condition (**Figure 3E-F, Figure 4C, Supplementary Figure 2.2D, Supplementary Figure 3.1D**).

One of the most differentially enriched transcripts in STB^{out} TOs was RYBP. (**Figure 4C-D**). RYBP contains chromatin remodeling activity as part of the PRC1 histone ubiquitination complex and can both increase and decrease the transcription of target genes (Rose et al., 2016; Silva et al., 2018). The expression dynamics of RYBP was directly correlated with the differentiation trajectory from CTB to STB, with upregulated expression beginning in CTB-pf (**Figure 4D**). We confirmed that RYBP protein is localized specifically to the nuclei of STB using immunofluorescence (IF) in STB^{out} TOs (**Figure 4E**). This revealed that RYBP expression was enriched in areas with high levels of CGBs, specific markers of the STB (**Figure 4E**). To validate STB-specific RYBP expression in placental tissue, we performed IF staining in full-term tissue sections, using E-cadherin as a marker of CTB and Cytokeratin-7 as a marker of CTB and STB cells. Consistent with TOs, RYBP protein exhibited STB-specific localization in tissue (**Figure 4F**) indicating that RYBP is a novel marker of STB differentiation, conserved in both TOs and full-term tissue.

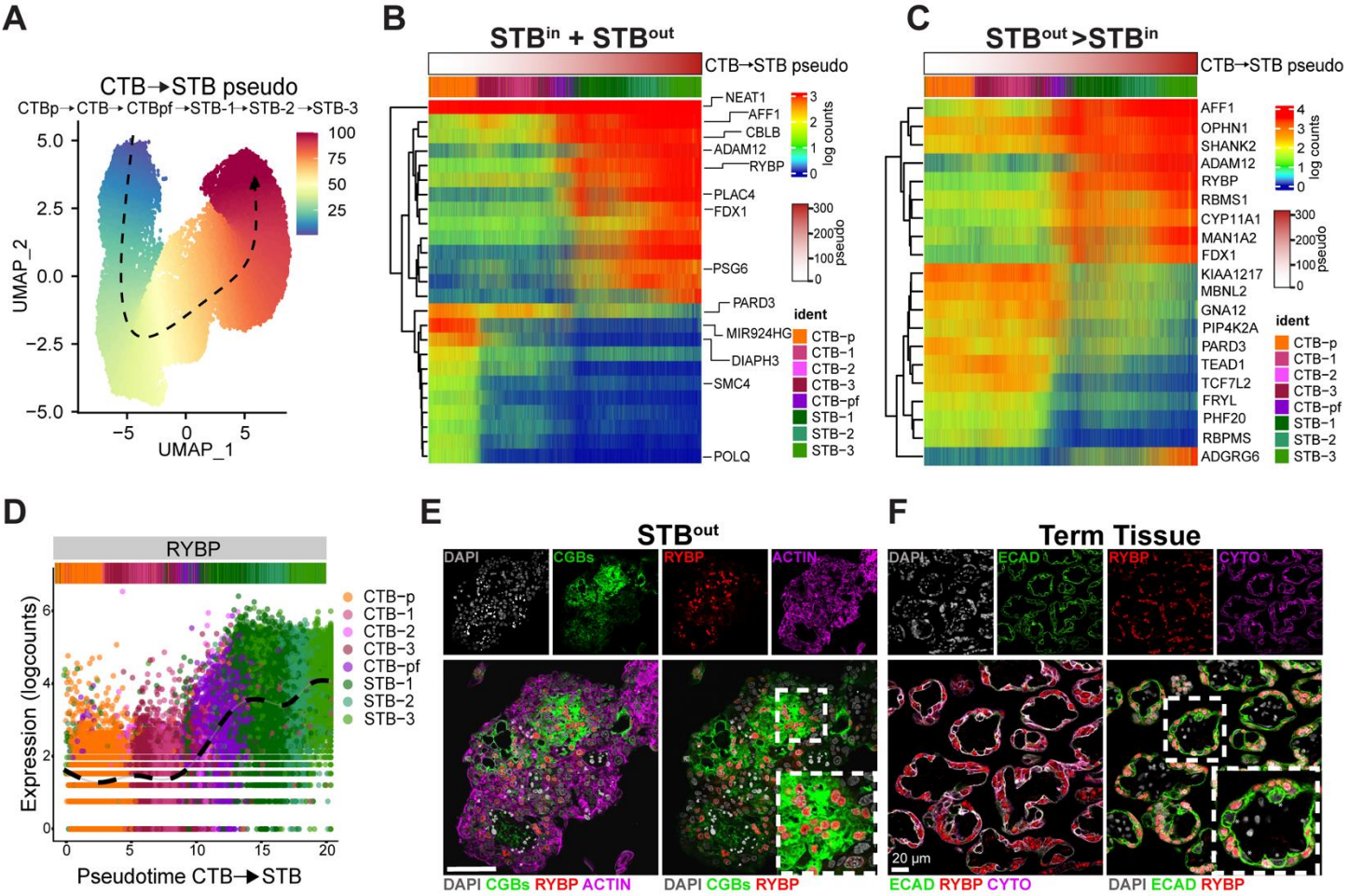

Figure 4: Pseudotime analysis of STB differentiation reveals STB-specific gene expression of RYBP. **A** Pseudotime was performed with Slingshot and assigned pseudotime value for each nucleus type is overlayed as a color scale on the UMAP from time 0 (blue) to time 100 (red). Arrow demonstrates directionality of the trajectory. Top genes associated with pseudotime (**B**) or enriched in STB^{out} compared to STB^{in} (**C**) are plotted on a barplot with nuclei ordered with the pseudotime seen in A. Logcounts and pseudotime are demonstrated as a color scale bar and the identity of each nucleus is labeled with a color as indicated in the legend. **D** The normalized expression of RYBP was plotted as a function of pseudotime for each nucleus in the STB^{in}+STB^{out} merged dataset. **E** Immunofluorescence of STB^{out} TOs was performed with chorionic gonadotropin (CGBs) and RYBP and stained with DAPI to label nuclei and Phalloidin to label Actin, which marks cell-boundaries. **F** Immunofluoresence of full-term tissue was performed with E-cadherin, RYBP and Cytokeratin-7 and stained with Hoescht to label nuclei. Stars in inlay represent CTB cells, as marked by E-cadherin, and are negative for RYBP.

Given the conservation of RYBP expression in TOs and tissue, we next sought to determine whether the CTB to STB trajectory in TOs was similar to that observed *in vivo*. To do this, we isolated the subset of nucleus types involved in STB differentiation (CTB, CTB-pf, and STBs) from full-term tissue, STB^{in}, and STB^{out} TOs and performed RNA velocity using spliced/unspliced matrices and plotted trajectories from each on a UMAP integrated for replicates of each sample type. This analysis creates a trajectory like slingshot but instead of accounting for pseudotime with bulk RNA expression, it leverages transcript splicing dynamics (Manno et al., 2018). The predominance of STB nuclei in the SN full-term tissue dataset precluded the ability to attain sufficient CTB-pf nuclei, but the velocity map demonstrated CTB differentiating into two STB lineages (**Figure 5A**, full-

term). Given the decreased STB:CTB ratios present in organoids, we were able to capture high numbers of CTB-pf nuclei and observed that this population is a precursor to the STB, as anticipated (**Figure 5A**, STB^{in} and STB^{out}). We then employed Velorama to infer gene regulation in these cells. Velorama is an RNA Velocity-based causal inference method that accounts for the multi-trajectory development of cellular state. It infers temporal causality on a directed acyclic graph where each node is a cell, and the edges indicate the velocity-implied direction of differentiation. Velorama derives gene regulatory networks by training a neural network to predict target gene expression profiles given regulator genes, such as transcription factors (TFs), and outputs an interaction score for every TF and target gene (TG) combination (Singh et al., 2024). Given the identification of the chromatin remodeler RYBP in the Slingshot analysis, we expanded Velorama to include other known chromatin remodelers (CRs), as they also have the potential to regulate gene expression levels.

To dissect the functional interactions between TF/CRs, we first compared the similarity of TGs interacting with each TF/CR and plotted this as a heatmap with a score of 1 indicating all TGs are shared and a score of 0 indicating no overlap (heatmap demonstrates high overlap in red and low overlap in blue, **Figure 5B**). In full-term tissue, these TF/CR fell into three modules that shared most target genes: 1- KMT2C/TBX3/AFF1/ZNF292, 2-ASH1L/RYBP, and 3-CEBPB/JUND/NCOA3 (**Figure 5B-5C**). In contrast to full-term tissue, most TGs in STB^{in} organoids were associated with AFF1/JUND/NOCA3/ZNF292/TBX3/CEBPB in no module order (**Figure 5B-5C**). Finally, STB^{out} appeared to have a similar distribution of TF/CRs as STB^{in}, apart from an increased prevalence of RYBP association with target genes in STB^{out} (**Figure 5B-5C**).

We next evaluated the specific TGs in each condition to predict the possible functions of the TF/CR and TG pairs. In full-term tissue, many STB-specific target genes were found to be associated using RNA velocity including CYP19A1, MFSD2A, ADAM12, PSGs, human placenta lactogen (CSH1), and the placenta specific insulin regulator PAPPA enriched in STB of full-term tissue (Wang et al., 2024). Module 3 was only associated with a handful of genes at full-term and with low interaction scores (interaction score demonstrated by arrow width). In contrast, Module 3 had a much stronger prevalence in both the number of target genes and interaction scores in both STB^{in} and STB^{out} organoids with some similar genes (conserved genes bolded, ADAM12, CYP19A1, PGF, PSG3) and some unique to organoids, particularly of note being hCG genes (CGA, CGB4, CGB7) (**Figure 5C**), whose expression is known to be decreased in the STB of full-term tissue (Rull and Laan, 2005). STB^{in} was the only condition to show a link between the TF/CRs and the VEGF receptor FLT1, consistent

with the enrichment of hypoxic/angiogenic associated genes in the STB-2 subtype of STB^{in} compared to STB^{out} (**Figure 3E, 5C**). Importantly, this analysis independently identified RYBP as a CR involved in the expression of STB TGs, consistent with our pseudotime analysis (**Figure 4B-D, 5B-C**). While RYBP was associated with most STB marker genes in full-term tissue and STB^{out}, it was associated with only a few TGs in STB^{in}. In fact, RYBP was associated with genes that were enriched in STB^{out} organoids in the Slingshot analysis (ADAM12 and MAN1A2) but not in STB^{in} TOs (**Figure 4B-C, 5C**), supporting the hypothesis that RYBP drives gene expression of a terminally differentiated STB subtype.

In summary, this gene network analysis suggests that many TF/CR and TG interactions are shared amongst tissue and TOs. However, many interactions in TOs also change as a function of culture condition. While module 3 is most linked to TGs expressed in TOs, RYBP is linked specifically to TGs expressed in tissue and STB^{out} TOs, but not STB^{in} TOs.

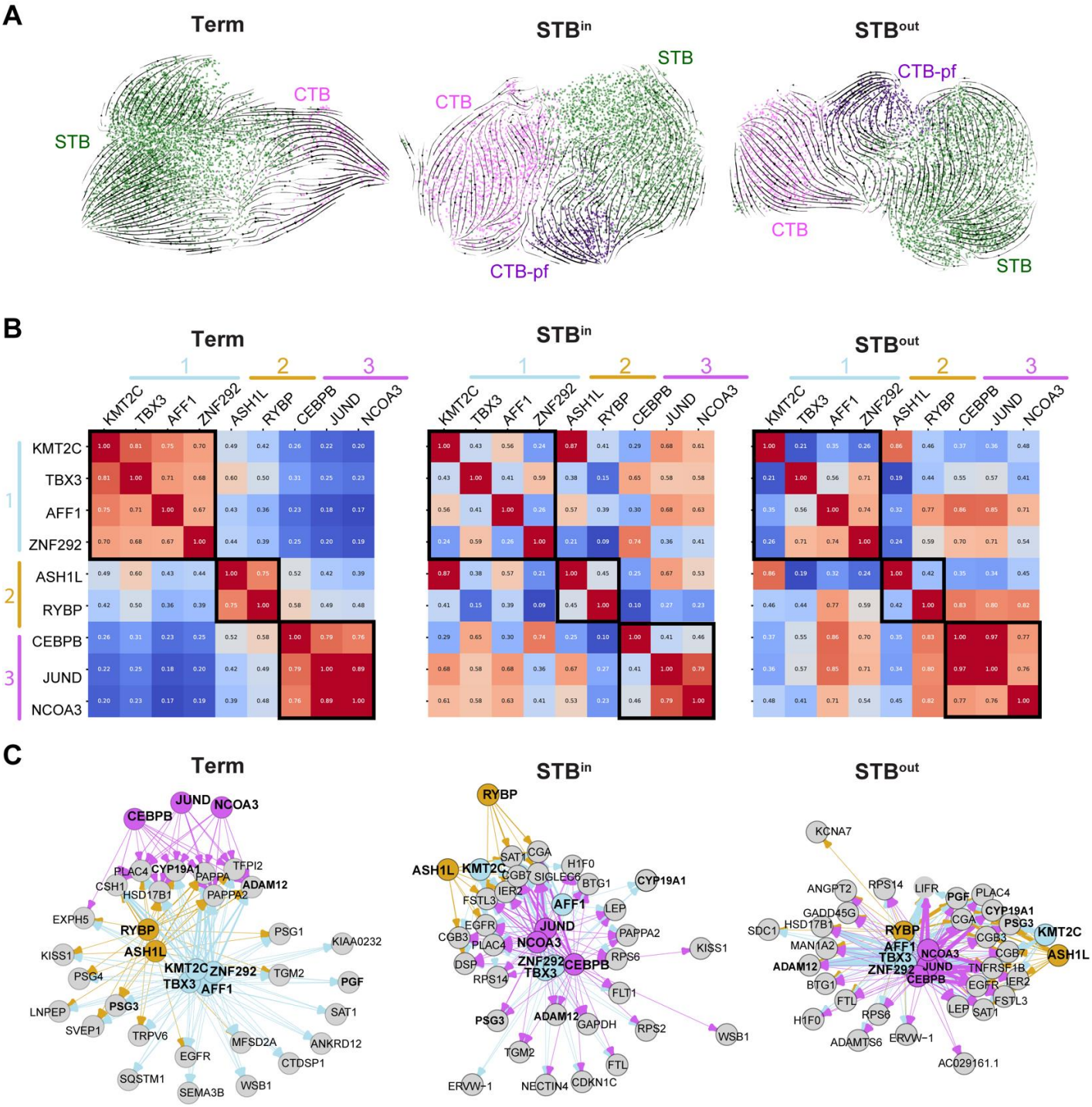

Figure 5 Gene regulatory network analysis reveals STB specific transcription factors conserved among term tissue and TOs. A Velocity derived from scVelo is visualized as streamlines on UMAP for either full-term tissue (Term), STB^{in}, or STB^{out} datasets. **B** TF/CR and TG pairs were identified via Velorama and plotted as a similarity matrix to show the overlap in TGs for each TF/CR. Each module discussed in the text is labeled as 1, 2, or 3. **C** Network graphs of TF/CRs and their respective TGs were plotted with igraph. Each TF/CR and respective arrows were false colored as per the module labels in B. The width of the arrow from each TF/CR to each TG represents the interaction strength score determined with Velorama.

Comparison of STB differentiation in TOs to first trimester and full-term placental tissue

Having identified several differences in STB differentiation between STB^{in} and STB^{out} TOs, we next sought to identify how these differences relate to placenta tissue across gestation. We used a publicly available first trimester SN sequencing dataset and integrated this data with the full-term tissue and TOs described above (**Supplemental Figure 6.1A**). Because tissue-derived datasets contain a large proportion of non-trophoblast nucleus types, we subset the integrated dataset to contain only trophoblasts in the STB lineage, which included both proliferating CTBs (CTB-p), CTBs (CTB-1 and CTB-2), pre-fusion CTBs (CTB-pf), and five distinct STB populations (**Figure 6A-6B**, **Supplemental Figure 6.1A-D**). The proportion of STB:CTB was higher in full-term tissue than in first trimester tissue (7:1 at full-term vs 1.5:1 in first trimester, combined dataset), as anticipated given the higher proportion of CTBs in first trimester (**Figure 6B**) (Benirschke et al., 2012; Mayhew, 2014). Of note, the STB:CTB ratios in TOs more closely resembled first trimester than term tissue in both culture conditions (1:1 for STB^{out} and 0.6:1 for STB^{in}) (**Figure 6B**). The tissue and TO samples exhibited dramatically different proportions of each CTB (CTB-1-2) subtype and each STB (STB1-5) subtype, which indicates sample to sample heterogeneity (**Figure 6A-B, Supplemental Figure 6.1A-C**). Therefore, we merged the two CTB and five STB populations together to globally detect the conserved and differentially expressed genes among the STB or CTB populations (**Figure 6C**). We first analyzed the expression of canonical marker genes for each nucleus type and found that each sample expressed these markers (**Figure 6D**), suggesting general conservation across both tissue types and TO conditions. To dissect what was different amongst the samples, we next analyzed the enriched genes in each nucleus type and identified GO terms associated with these genes for each sample type (**Figure 6E and Supplemental Figure 6.1E**). GO terms associated with the CTB populations were remarkably conserved amongst all sample types (**Supplemental Figure 6E**). In contrast, STB exhibited greater diversity of functions between sample types (**Figure 6E**). While GO terms involved in ER to Golgi transport and hormone production were conserved in all STB samples, many processes were found only within a subset of sample types (**Figure 6E**). For example, genes with ER stress, ER associated degradation, and macroautophagy GO terms were expressed in TOs but not in tissue. In contrast, GTPase signaling and vesicle organization were present in first trimester, term, and STB^{out} TOs, but not in STB^{in} (**Figure 6E**). Together, these findings suggest that the STB exhibits greater heterogeneity in function across sample types than do CTBs.

To determine what genes were significantly different in each sample, we performed pseudobulk analyses using DESeq2, plotted genes on a Volcano plot, and colored genes significantly associated with different GO terms (**Figure 6F**). We performed this analysis comparing STB in either first trimester tissue to TOs (STB^{out} or STB^{in}) or full-term tissue to TOs (STB^{out} or STB^{in}) (**Figure 6F**). Many GO terms were enriched across all comparisons. This included an increase in extracellular matrix, cell substrate adhesion, and connective tissue development genes within the tissue datasets, with a particular enrichment of collagen genes and matrix metalloproteases (ADAM and MMP family members) (**Figure 6F**) (Qu and Khalil, 2022). In contrast, the STB present in organoids exhibited an enrichment of genes involved in cytoplasmic translation/ ribosome biogenesis as well as oxidative phosphorylation/ DNA damage (**Figure 6F**). In addition, genes associated with cytokine production and the immune response based on GO terms were present in full-term tissue but not first trimester tissue or TOs (**Figure 6F**). Therefore, while STB of TOs and tissue share many conserved marker genes, a subset of STB gene expression is differentially regulated between tissue and TOs.

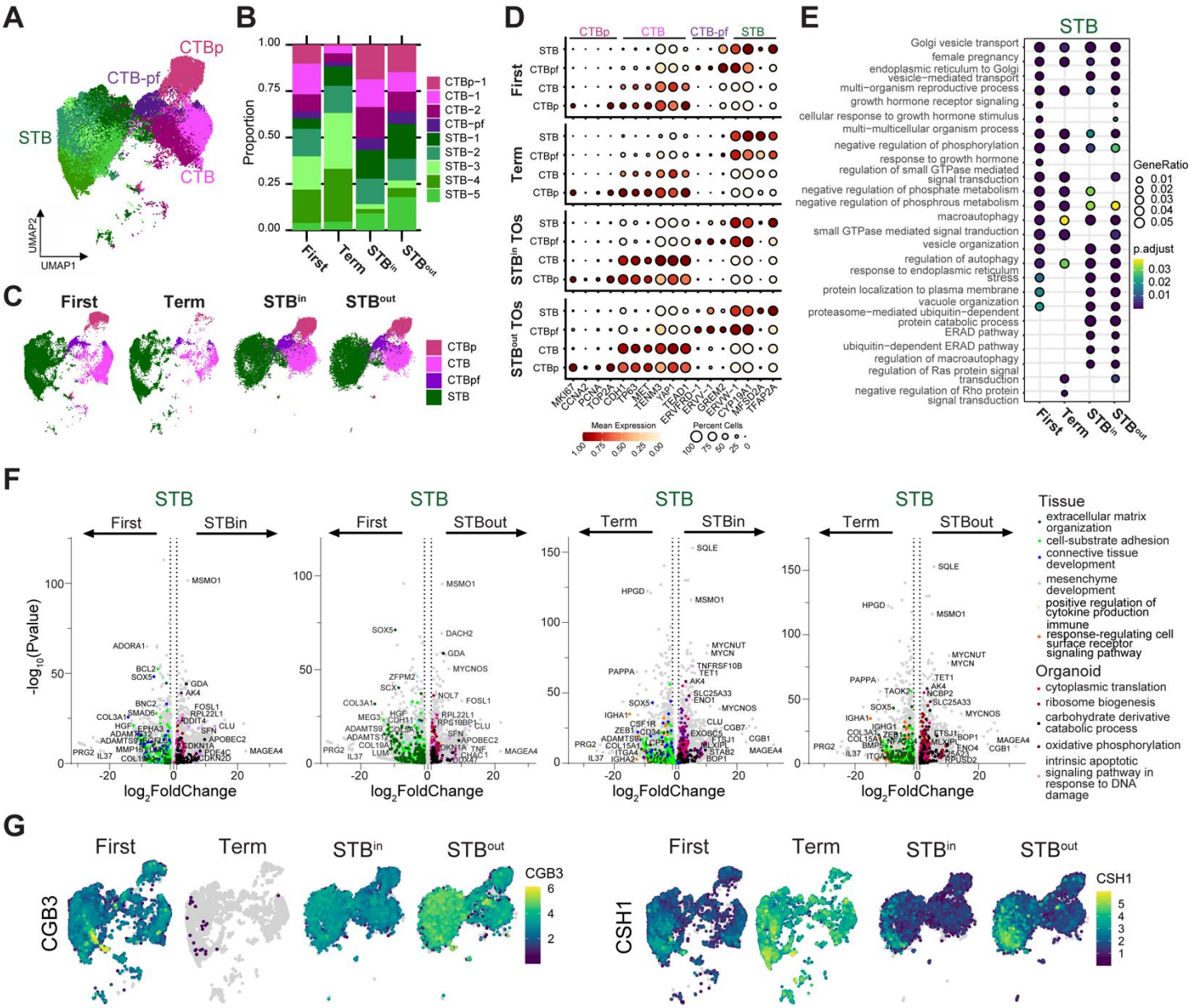

Figure 6: Similarities and differences between STB in first trimester and full-term tissue and TOs. A UMAP of the integrated SN dataset including first trimester, full-term tissue, STB^{in} TOs, and STB^{out} TOs. **B** Relative proportion of each nucleus type for each sample in the integrated dataset in A. **C** UMAP of the integrated dataset split by sample type. The five STB subtypes were merged into a single STB subtype while the two non-proliferative CTB subtypes were merged. **D** Dot plot of key trophoblast marker genes in the STB lineage with heatmap representing mean gene expression and size of the dot representing the percent of nuclei expressing each marker. The labels on the top of the graph refer to the established marker genes used to identify the identity of each cluster. **E** The top DEG in the STB of each sample type were analyzed for biological process GO term enrichment with clusterProfiler and plotted as a dotplot. **F** DEseq2 was used to find DEGs between different sample types for the merged STB cluster. GO terms for DEGs enriched in each sample type were found with ClusterProfiler and colored on the UMAP with select representative genes highlighted in text. **G** Feature plots demonstrating RNA expression of selected genes.

We next evaluated the expression of genes known to change throughout gestation in each sample type. For example, many hormones are differentially released throughout pregnancy with first trimester tissue exhibiting high hCG production (CGB genes) and full-term tissue releasing more human placenta lactogen (CSH

genes) (Costa, 2016; Rull and Laan, 2005; SAMAAN et al., 1966). Consistent with these gestational hormone trends, STB from first trimester expressed hCG genes while there was no expression in full-term tissue (**Figure 6G, Supplemental Figure 6.1F**). Further, full-term tissue exhibited an increase in CSH1 expression compared to first trimester (**Figure 6G, Supplemental Figure 6.1F**). STB^{in} and STB^{out} TOs expressed both hormones in the STB suggesting organoids can produce hormones differentially expressed throughout gestation (**Figure 6G, Supplemental Figure 6.1F**). STB^{out} TOs exhibited an increase in expression of both hormones compared to STB^{in} TOs, consistent with a higher proportion of terminally-differentiated, hormone expressing nuclei (**Figure 6G, Supplemental Figure 6.1F**). Consistent with previous reports, there was an increase in the expression of FLT1 and decrease in PAPPA in the STB of first trimester compared to full-term tissue, with TOs resembling first trimester expression (**Supplemental Figure 6.1G-H)** (Wang et al., 2024). Together, these results demonstrate that while the STB of each sample expresses key STB marker genes, both gestational age and trophoblast organoid culture conditions can modify the gene expression patterns of the STB.

Discussion

A critical barrier to understanding human gestation has been the limited number of accessible models for the placenta. In this study, we conducted comparative SC and SN RNA sequencing on full-term placenta tissue and TOs. Our findings demonstrate that SN sequencing is crucial for capturing the STB lineage due to its distinct syncytial structure. We characterized the nucleus types in each TO model and utilized DEG and pseudotime analyses to define three STB subtypes present in both STB^{in} and STB^{out} TOs, albeit at different ratios. These include a juvenile population that exhibited intermediate CTB and STB expression (STB-1), an FLT1+ population enriched in genes involved in oxygen sensing and the stress response (STB-2), and a fully differentiated subtype enriched in transport and GTPase signaling molecules (STB-3). We identified the chromatin remodeler RYBP as a gene linked to STB differentiation that exhibits STB-specific protein expression and gene regulatory analysis suggests that RYBP may be involved in the terminal differentiation of STB nuclei. Finally, we compared STB gene expression between placental tissues from first trimester and full-term to TOs. This showed that although standard STB differentiation markers are maintained in all, there is substantial heterogeneity in STB gene expression between the different sample types. Together, these results draw important implications for our understanding of STB nuclear differentiation and show how TOs can serve as relevant STB models.

STB^{out} TOs grown in suspension maintain native polarity and exhibit an increase in syncytia size, with >50 nuclei/syncytia in STB^{out} compared to ~10 nuclei/syncytia under standard STB^{in} culture conditions (Yang et al., 2023). However, it was unknown whether CTB grown via this method maintained their proliferative capacity. Here we show that the proportion of mitotic cells remains constant between TOs grown in STB^{in} and STB^{out} conditions, suggesting culture in suspension is not a terminal, post-mitotic state. In fact, the proportion of STB nuclei increased in the STB^{out} condition was concurrent with a decrease in the CTB-CC population. *In vivo*, CTB-CC cells sit adjacent to the villous trees and maternal uterus and are thought to progressively differentiate into EVT cells that then can invade into the uterus (Arutyunyan et al., 2023; Boyd and Hamilton, 1970; Turco and Moffett, 2019). Therefore, the increase of STB in the STB^{out} condition could be caused by promotion of STB lineage and an inhibition of differentiation down a CTB-CC or EVT lineage.

The enrichment of STB nuclei in SN sequencing allowed us to identify and define three populations of STB in the STB^{in} and STB^{out} TO conditions. STB-1 represented a juvenile population undergoing a transition from CTB to STB gene expression. These nuclei may have recently incorporated into the syncytia and are actively undergoing differentiation at the time of sequencing. STB-2 expressed the VEGF receptor FLT1 and is

enriched in genes involved in responding to oxygen levels and ER stress, suggesting STB-2 might play a role in responding to low oxygen levels. Finally, STB-3 represents the terminal differential state of STB based on the pseudotime trajectory and exhibits an increase in a subset of STB markers, GTPase signaling molecules, and transporter proteins. Importantly, culture conditions changed the relative enrichment of these subtypes. Whereas STB^{in} TOs were enriched for the juvenile STB-1 and oxygen sensing STB-2 populations, STB^{out} TOs have an increased proportion of the terminally differentiated STB-3 subtype. Future studies dissecting how culture of TOs in either extracellular matrix or suspension impacts environmental cues like oxygen concentrations, cell tension, and media flow dynamics will help elucidate the molecular mechanism driving these different STB subtypes. Of note, these three STB subtypes are remarkably like those recently defined in first trimester and full-term tissue: a juvenile population, a FLT1 expressing population enriched in genes involved in oxygen sensing, and a PAPPA positive population that expresses GTPase signaling molecules and hormones (Wang et al., 2024). This resemblance suggests TOs can recapitulate similar nucleus subtypes as those seen *in vivo*, indicating their strength as an experimental model.

How might these distinct nuclear transcriptional identities affect the function of the STB? Despite the STB being one large cytoplasm where molecules can freely mix by diffusion, it has long been suggested to contain distinct cytoplasmic zones that specialize in different functions (Benirschke et al., 2012; Burgos and Rodríguez, 1966; Burton, 1990). For example, STB cytoplasmic regions adjacent to the fetal vasculature dramatically thin to facilitate diffusional exchange and express angiogenic promoting proteins while regions where hormones are produced will exhibit dense packing of cytoplasmic organelles and express hormone and protein trafficking molecules (Baczyk et al., 2004; Beck et al., 1986; Burton and Jauniaux, 1995; Clark et al., 1998; Hempstock et al., 2003; Jauniaux et al., 2003; Khaliq et al., 2009; Morrish and Marusyk, 1997; Mouzon, 1997; Sharkey et al., 1993). One potential mechanism for creating these distinct cytoplasmic zones is nuclear specialization, whereby individual nucleus identities might be spatially localized to different cytoplasmic regions, as has been demonstrated for nuclei in syncytial muscle fibers (Kim et al., 2020). Different nuclear identities likely arise from a combination of differentiation pathways and environmental cues. The generation of an organoid cell culture model that recapitulates the STB nuclear identities seen *in vivo* is a critical stride towards deciphering the mechanisms that allow the giant STB cell to effectively carry out its many essential functions.

To dissect the transcription factors that drive STB differentiation we applied gene regulatory analysis and identified multiple TF/CR modules potentially involved in differentiation of STB in full-term tissue and TOs. Interestingly, the module most associated with STB^{in} included the TF CEBPB, which is important for placenta development in mice and was recently found to be involved in STB differentiation in first trimester but not in full-term tissue (Bégay et al., 2004; Wang et al., 2024). Consistent with these results, we found that the TF CEBPB was only associated with a few genes in our independent full-term tissue dataset, suggesting that STB of TOs might employ transcriptional programs characteristic of the first trimester. The final module includes the CR RYBP, which is involved in a non-canonical form of the PRC1 polycomb complex that ubiquitinylates histones and can modulate gene expression (Rose et al., 2016; Silva et al., 2018). We found that STB^{out} TOs and full-term tissue exhibited more TGs predicted to be controlled by RYBP compared to STB^{in} TOs. Given the increased proportion of hormone expressing nuclei in full-term tissue and STB^{out} TOs, we speculate that RYBP might be involved in terminal differentiation of STB. Of note, RYBP deletion in mice is embryonic lethal due in part to a failure to form trophectoderm and subsequent invasion defects (Pirity et al., 2005), consistent with a possible role of RYBP on STB differentiation in human placenta.

While the global subtypes found in first trimester, full-term tissue, STB^{in} TOs, and STB^{out} TOs were similar, many genes were differentially expressed in each STB population. One significant difference between the STB of full-term tissue and TOs was in hormone expression. It has long been appreciated that the STB differentially expresses hormones as a function of gestational age (Costa, 2016; Kumar and Magon, 2012), but it was not known 1- how TOs mirror this expression and 2- how isolation of TOs from different stages of tissue gestation affected expression. We found that while the TOs used in this study were derived from full-term CTBs, the STB associated with these organoids express hormone transcripts classically associated with early gestation. This suggests that the cues that restrict these hormones to different gestational stages *in vivo* are not intrinsic to the isolated CTBs and can be studied in full-term derived TOs. Future work adding maternal cues to the TO system will help define how STB hormone levels are mechanistically modulated.

In conclusion, our study elucidates STB nucleus subtypes in TOs, tracks their proportions across culture conditions, and compares gene expression to STB *in vivo*. The fluctuating proportions of STB subtypes across TO culture conditions imply that environmental cues can direct individual nuclei in the same cell into different identities. These findings underscore the power of TOs as an experimental model for studying the STB.

Methods:

Tissue Processing for SC and SN sequencing

Placenta tissue was collected from patients undergoing scheduled C-sections at UNC Health consented under IRB 21-2055. Patient information, sequencing data, and tissue samples from these experiments was later transferred to Duke under the IRB Pro00113088. Immediately after placenta delivery a cotyledon from the center of the placenta was dissected. Samples from both decidua and villous tissue were snap frozen in liquid nitrogen for future processing within ten minutes of placenta delivery to minimize STB degradation. Additional samples were fixed in 10% buffered formalin for subsequent tissue paraffin embedding and slicing. The remaining villous/decidua tissue from the dissected cotyledon was then immediately processed into single cells, as described below. A list of the tissues used in this study is available in **Supplementary Table 1**.

SC processing: The cotyledon (decidua + villous, chorion removed) was chopped into fine pieces (<1mm) with a scalpel and washed with 1x PBS in cheese cloth until flow through was clear of blood. Tissue was placed into Trypsin media (1X PBS without calcium or magnesium, 0.2% Trypsin (Thermo 15090046), 0.53M EDTA) and incubated at 37°C for ten minutes in a shaking water bath. After incubation trypsin was inactivated with 100mLs of Wash Media (DMEM F12 media + 20% FBS). Supernatant was passed through a sterile cheese cloth, spun down, and resuspended to Resuspension Media (DMEM F12 media + 10% FBS). Remaining tissue was then placed into 25mL collagenase buffer (1mg/mL collagenase V (Sigma C9263) in Wash Media) and shaken at 37°C for ten minutes. Supernatant was passed through cheese cloth, spun down, and resuspended in Resuspension Media. Cell pellets from both digestion steps were combined and pelleted, resuspension media removed, and resuspended in 10mLs RBC lysis buffer (Thermo 00-4333-57) and incubated at RT for 10min. Cells were passed through a 100µm filter, spun down, and passed through a Milltenyi Debris Removal Solution (130-109-398) gradient as per the manufacturer's instructions. The final pellet was then resuspended in 1X PBS + 0.04% BSA (Sigma A1595).

SN processing: Single nuclei were isolated with the 10X Chromium Nuclear Isolation Kit (CG000505) as per the User Guide with the following changes. 50mgs of frozen tissue was resuspended in lysis buffer on ice, dounced to homogenize, and incubated for a total of only 7 minutes from the resuspension step to centrifugation. In addition, while the initial centrifugation step in lysis buffer was performed at 500xg for 5 min to minimize time

spent in lysis buffer, subsequent wash spins were done at 500xg for 10min to minimize loss. The final pellet was then resuspended in 1X PBS + 0.04% BSA (Sigma A1595) +10X Genomics supplied RNAse inhibitor.

Organoid Culture

STB^{in}, STB^{out}, and EVT^{enrich} TOs were derived, propagated, and differentiated as described previously (Yang et al., 2022 and 2023). Briefly, STB^{in} TOs were derived and maintained by sequential digestion of term placental chorionic villi with 0.2% trypsin-250 (Alfa Aesar, J63993), 0.02% EDTA (Sigma-Aldrich, E9884), and 1.0 mg/mL collagenase V (STEMCELL Technologies, 100-0681), followed by further mechanical disruption by pipetting. Pooled digests were washed with Advanced DMEM/F12 medium (Gibco 12634-010) and pelleted by centrifugation, then resuspended in ice-cold Matrigel (Corning 356231). Matrigel "domes" (40 µl/well) were plated into 24-well tissue culture plates (Corning 3526) and overlaid with 500 µL prewarmed term trophoblast organoid medium (tTOM) (**Supplementary Table 3**). Cultures were maintained in 37ºC humidified incubator with 5% CO_2. Medium was renewed every 2-3 days. To generate STB^{out} TOs, mature STB^{in} TOs were released from Matrigel domes with cell recovery solution (Corning, 354253) on ice for 30-60min, pelleted, washed one time with cold basal media (Advanced DMEM/F12 + 1% P/S + 1% L-glutamine + 1% HEPES), and then resuspended in pre-warmed tTOM supplemented with 5 µM Y-27632, and transferred into an ultra-low attachment 24-well plate (Corning 3473) for suspension culture at 37℃ and 5% CO2 for 48 hours. To generate EVT^{enrich} TOs, established STB^{in} TOs were passaged into new Matrigel "domes" as described above and previously (Yang et al., 2022 eLife), and maintained in tTOM for ~ 5 days prior to switching to EVT differentiation media 1 (EVT m1 recipe: **Supplementary Table 4**) for 9 days culture, then replaced with EVT m2 with the same recipe as EVT m1, but lacking NRG1 for a further 3-4 days. A list of the TOs lines used in this study is available in **Supplementary Table 1**.

Organoid Processing for SC and SN sequencing

STB^{in} TOs were processed into both single cells and nuclei for SC/SN sequencing while STB^{out} and EVT^{enrich} TOs were processed into single nuclei for SN sequencing via the following protocols.

<u>SC processing:</u> STB^{in} TOs were dissociated by scraping Matrigel domes into 1 mL of pre-warmed TrypLE Express (Invitrogen, 12605036) and incubating at 37ºC for 12 min, swirling the tube every 2-3 min. Dissociated organoids were pelleted at 1250 rpm for 3 min and re-suspended in 200 µL DMEM containing 10% FBS. Resuspended organoids were subjected to vigorous manual disruption using a single channel p200 pipette

(Ranin, 17008652) for 3 min followed by the addition of 800 µL of DMEM containing 10% FBS. The disrupted suspension was then passed over a 40 µm filter cell strainer (Corning, 352098). Flow through was then centrifuged at 1250 rpm for 5min and the pellet resuspended in 250 µL of 1x PBS for a final volume of ~300 µL and cell counts of ~1 x 10^6 cells/mL.

SN processing: TOs from each condition (STB^{in}, STB^{out}, EVT^{enrich}) were harvested by scraping with a wide bore pipette, centrifuged to pellet (600xg for 6min), resuspended in 100uls TrypLE (Thermo Fisher, 12605010), and incubated at 37ºC for 10min. After incubation each sample was pipetted 100x with a P200 pipette to dissociate cells and placed on ice. Single nuclei were then isolated with the 10x Chromium Nuclear Isolation Kit (CG000505) as per the User Guide with the following changes. 500uls of Lysis buffer was added to the TO/TrypLE solution and transferred to a 2mL Kimble Dounce (Millipore Sigma, D8938) on ice, dounced 10x, and subsequently incubated on ice for a total of 10 minutes. Remaining steps were performed as suggested, except for final wash step spins were performed at 500xg for 10min to minimize nuclei loss. The final pellet was then resuspended in 10mLs of 1X PBS + 0.04% BSA (Sigma A1595) +10X Genomiocs supplied RNAse inhibitor, nuclei counted, and 10,000 nuclei run in each well of a chromium controller.

10X Genomics library generation, sequencing, and data analysis

SC suspensions were stained with Trypan Blue and counted to obtain live/dead cell ratios while SN were stained with Ethidium Homodimer-1 (Thermo E1169) and counted with a hemocytometer on a fluorescent microscope. 10,000 SC/SN of each sample type were loaded into individual chip wells and run on a 10x chromium controller with the Chromium Single Cell 3' Reagent Reagent Kit v3.1 (Dual Index) following the manufacturers protocol. Tissue libraries were then sequenced on an Illumina NovaSeq S2 at a targeted sequencing depth of 100,000 reads/cell or nucleus while organoid libraries were sequenced on an Illumna NovaSeq S4 at a targeted sequencing depth of 74,000 reads/cell or nucleus. Cell Ranger was then used to align reads to the human genome (GRCh38) and create a counts matrix.

SC and SN Data Analysis: Post-processing, quality control, and read alignment to the hg38 human reference genome were performed using 10x CellRanger package (v6.1.2, 10x Genomics). Gene expression matrices generated by the 10x CellRanger aggregate option were analyzed using Seurat (version 4.0) in R (Butler *et al.*, 2018; Hao *et al.*, 2021; Satija *et al.*, 2015; Stuart *et al.*, 2019). For SC, cells with at least 200 and no more than 10,000 unique expressed genes were included in downstream analysis, and cells with more than 25%

mitochondrial reads were excluded from analysis. For SN, nuclei with at least 800 and no more than 10,000 unique features and less than 60,000 counts were included in downstream analysis, and nuclei with more than 7.5% mitochondrial reads and 3% ribosomal reads were excluded from analysis. To eliminate batch effects, datasets from unique donors were normalized using the *sctransform* function (version 2) and integrated using the *FindIntegrationAnchors()* in Seurat (version 4.0) in R (Stuart *et al.*, 2019). Variables regressed included nFeatures, nCounts, percent mitochondria and ribosomes, and X- and Y-linked genes to avoid sex-associated differences. Dimensional reduction was performed using the *RunPCA()* function to obtain the first 40 principal components, which was determined using *ElbowPlots()* across the first 50 dimensions. To identify clusters, Louvain clustering (Seurat *FindClusters()* function) was performed, and optimal resolution was determined using the *clustree()* function (Zappia and Oshlack, 2018) on a range of resolutions between 0.2-1.0, with 0.6 selected for TOs and 0.3 selected for tissue. To identify clusters enriched in combined files of TOs and tissue, dataset integration was performed using Harmony and Louvain clustering (Seurat) performed at a 0.3 resolution, as optimized using *clustree()* (Zappia and Oshlack, 2018). Differential expression analysis between clusters was performed using the Wilcoxon rank sum test (Seurat) using *FindAllMarkers()*, with genes with a $\log_2$ fold change threshold set to 0.25 and FDR-adjusted p-value < 0.05 considered significant. Pseudobulk differential expression analysis was performed using DESeq2 (Love et al,). GO term enrichment was performed with clusterProfiler using *compareCluster.*

<u>Pseudotime:</u> The *slingshot* package (version 2.6.0) in R was used to determine differentiation trajectories from clusters identified in Seurat with unbiased starting and ending roots (Street *et al.*, 2018). The raw counts and above-generated slingshot object were used to run *evaluateK()* with the total number of knots ranging from 3 to 9. The optimal number of knots was determined to be 5. The *fitGAM()* function using *tradeSeq* (1.5.10) was run with this resulting value and gene expression along lineages identified using the *associationTest()* function (Van den Berge *et al.*, 2020). Heatmaps of expression changes across lineages were generated using *ComplexHeatmap()* on log transformed counts and rasterized using the *ImageMagick* "Bessel" filter (ImageMagick, 2023). The *plotGenePseudotime()* function was used to visualize raw count gene expression in individual cells across lineages from the *slingshot* object.

<u>RNA Velocity and Velorama:</u> RNA velocity was performed via the python based program scVelo on snRNAseq data from both placenta tissues of three patients and organoids from three patient-derived TO cell lines (Bergen

et al., 2020). The organoids were further divided into STB^{in} and STB^{out} subcategories, resulting in nine total datasets in our analysis. First, we generated UMAPs for each data source (full-term tissue, STB^{in}, and STB^{out}) with corresponding trajectory vectors. For the TOs we included only the CTB, CTB-pf, and STB nucleus types in the analysis. For each data source, the sample datasets were integrated with Scanorama to eliminate dataset-specific batch effects for transcript counts as well as spliced and unspliced transcripts (Hie et al., 2018). The samples were then merged and UMAPs with trajectory vectors were created using the scVelo library. Then, we employed Geosketch to downsample the cell population represented in the UMAP while preserving transcriptomic heterogeneity (Hie et al., 2019). This was done to enhance the clarity and distinction of cells on the UMAP. Second, we inferred gene regulatory networks with Velorama (Singh et al., 2024). We compiled lists of human transcription factors (TFs) and genes coding for chromatin remodelers (CRs) from sources like https://www.factorbook.org/tf/human to use as regulatory genes, along with a selection of highly variable genes and genes of interest from the tissue and organoid datasets to use as our target genes. Velorama was then used to infer the gene regulatory networks under default settings and produced a total of nine regulatory-target gene interaction matrices for tissues and organoids raw data sets. Each interaction matrix provides scores that highlight the strength of the relationship between specific regulatory-target gene pairs. We then ranked the regulatory-target gene pairs by their interaction strength and identified top TFs in each sample, after filtering TFs by number of target genes among the top 500 pairs. Heatmaps were then created based on the overlap of target genes with a score of 1 representing total overlap and a score of 0 indicating no overlap. Finally, top target genes in each cluster were found via sorting by interaction score and plotted as a network analysis with the R package igraph, with the width of the arrow representing the Velorama interaction strength score.

Immunofluorescence in placenta tissue

FFPE tissue sections derived from the same patients sequenced in Figure 1 were removed from paraffin and rehydrated via an iteration through the following 3min wash steps (Xylene, Xylene, 1:1 Xylene:100% EtOH, 100% EtOH, 100% EtOH, 95% EtOH, 70% EtOH, 50% EtOH). Slides were then placed under running tap water for 5 minutes to re-hydrate then transferred to sodium citrate buffer (10mM sodium citrate, 0.05% Tween 20, pH6) and placed into boiling water for 20min for antigen revival. Slides were then placed under running tap water for 10minutes then transferred into PBS. To perform IF, tissue was permeabilized with 0.5% Triton X-100 in 1X PBS for 20min at RT then washed 2x in 1X PBS. Reb blood cell autofluorescence was quenched with TrueBlack

Lipofuscin Autofluorescence Quencher (Biotium #2300) as per the manufacturer's instructions then washed 2x in 1X PBS. Tissue slides were then blocked in blocking buffer (1% BSA in 1X PBS) for 1 hour at RT. Primary antibodies were then incubated overnight at 4℃ in 0.1% BSA in 1x PBS in the following dilutions: 1:1000 RYBP (Millipore Sigma HPA053357), 1:500 Cytokeratin-7 (Millipore Sigma MABT1490), and 1:200 E-cadherin (BD Biosciences 610181). Slides were rinsed 2x in 1X PBS, and incubated in secondary antibodies for 1 hour at 37℃ (Invitrogen A-21247, A-11011, A-11001). Slides were rinsed 2x in 1X PBS, incubated in 1 µg/ml Hoechst in 1X PBS for ten minutes at RT, and finally washed 1x in 1X PBS. PBS was then removed and slides mounted with ProLong Diamond Antifade (Thermo P36965) and dried overnight prior to imaging. Slides were imaged on a Nikon Ti-E stand equipped with a Yokogawa CSU-W1 spinnig disk confocal unit with a 40x/1.25NA Nikon Silicone objective and illuminated with 405/488/565/646 laser sources.

Cryosectioning and immunofluorescence staining in TOs

STB^{out} TOs were collected from suspension culture by gravity in microcentrifuges tubes pre-coated with regular FBS, then rinsed once with 1 × PBS prior to fixing in 4% PFA at RT for 2 h. Pelleted TOs were washed twice with 1 × PBS and resuspended in 1 × PBS with 0.5 mL 20% (wt/vol) sucrose solution per sample, then transferred to 4℃ overnight to allow all the organoid units to pellet into the bottom of sucrose solution. On the following day, 7.5% gelatin (wt/vol)/10% (wt/vol) sucrose embedding solution was pre-warmed at 37℃ for 30 min, then organoid units were isolated from sucrose solution into small size molds (7×7×5 mm) and polymerize with embedding solution at 4 ℃ for 20 min before transferring into -80 ℃ for at least 3 hrs prior to cryosectioning.

To section above prepared organoid frozen blocks, the blocks were transferred from -80℃ into the cryosection machine (Leica CM1950 Cryostat) at -20℃ to equilibrate for 15 min, then 10 µm thickness sections cut. The cryosections were incubated at RT for 15 min before incubation in permeabilization buffer (5% <wt/vol> goat serum/0.5% <vol/vol> Trition X-100 in 1 × PBS) for 45 min at RT. Cryosections were washed and blocked in 5%(v/v) goat serum/0.1%(v/v) Tween-20 in PBS for 15 min at RT and then incubated with rabbit anti-human RYBP polyclonal antibody (Sigma, HPA053357) and mouse anti-human hCG-β antibody (abcam, ab9582) diluted in above-described blocking solution at 4℃ overnight. The following day cryosections were washed with 1 × PBS and then incubated for 1 h at RT with Multi-rAb CoraLite Plus 488 Goat anti-mouse (Proteintech, RGAM002) and Multi-rAb CoraLite Plus 594 Goat anti-rabbit (Proteintech, RGAR004) recombinant secondary antibodies, and Alexa Fluor 647–conjugated phalloidin (Invitrogen, A22287). Cryosections were washed again

with 1 × PBS and mounted in Vectashield (Vector Laboratories, H-1200) containing 4′,6-diamidino- 2-phenylindole (DAPI). Images were captured using a Olympus Fluoview FV3000 inverted confocal microscope and contrast-adjusted in Photoshop or Fiji.

Acknowledgements

We thank Jennifer Gilner, Jillian Hurst, and the Project Hope1000 (Duke University) for providing placental tissue used to derive organoids in this work. We thank Karen Dorman, Neeta Vora, Charles Perou, and Michelle Hayward at UNC Chapel Hill for their assistance in obtaining IRB approval and placenta tissues at UNC CH. This project was supported by NIH AI145828 (CBC), an HHMI Faculty Scholar award (ASG), NSF 743900 (ASG). The organoid work performed by MMK was supported by NIH K00CA245719. We thank the Duke University School of Medicine for the use of the Sequencing and Genomic Technologies Shared Resource and the Translational Genomics Lab at UNC Chapel Hill Lineberger Comprhensive Cancer Center, both of which provided RNA-seq services.

Bibliography

Aghababaei, M., Hogg, K., Perdu, S., Robinson, W.P., Beristain, A.G., 2015. ADAM12-directed ectodomain shedding of E-cadherin potentiates trophoblast fusion. Cell Death Differ. 22, 1970–1984. https://doi.org/10.1038/cdd.2015.44

Arutyunyan, A., Roberts, K., Troulé, K., Wong, F.C.K., Sheridan, M.A., Kats, I., Garcia-Alonso, L., Velten, B., Hoo, R., Ruiz-Morales, E.R., Sancho-Serra, C., Shilts, J., Handfield, L.-F., Marconato, L., Tuck, E., Gardner, L., Mazzeo, C.I., Li, Q., Kelava, I., Wright, G.J., Prigmore, E., Teichmann, S.A., Bayraktar, O.A., Moffett, A., Stegle, O., Turco, M.Y., Vento-Tormo, R., 2023. Spatial multiomics map of trophoblast development in early pregnancy. Nature 616, 143–151. https://doi.org/10.1038/s41586-023-05869-0

Aye, I.L.M.H., Aiken, C.E., Charnock-Jones, D.S., Smith, G.C.S., 2022. Placental energy metabolism in health and disease—significance of development and implications for preeclampsia. Am. J. Obstet. Gynecol. 226, S928–S944. https://doi.org/10.1016/j.ajog.2020.11.005

Baczyk, D., Satkunaratnam, A., Nait-Oumesmar, B., Huppertz, B., Cross, J.C., Kingdom, J.C.P., 2004. Complex Patterns of GCM1 mRNA and Protein in Villous and Extravillous Trophoblast Cells of the Human Placenta. Placenta 25, 553–559. https://doi.org/10.1016/j.placenta.2003.12.004

Bai, X., Lenhart, K.C., Bird, K.E., Suen, A.A., Rojas, M., Kakoki, M., Li, F., Smithies, O., Mack, C.P., Taylor, J.M., 2013. The smooth muscle-selective RhoGAP GRAF3 is a critical regulator of vascular tone and hypertension. Nat. Commun. 4, 2910–2910. https://doi.org/10.1038/ncomms3910

Barker, S.B., Cumming, G., Horsfield, K., 1973. Quantitative morphometry of the branching structure of trees. J. Theor. Biol. 40, 33–43. https://doi.org/10.1016/0022-5193(73)90163-x

Barrios, V., Chowen, J.A., Martín-Rivada, Á., Guerra-Cantera, S., Pozo, J., Yakar, S., Rosenfeld, R.G., Pérez-Jurado, L.A., Suárez, J., Argente, J., 2021. Pregnancy-Associated Plasma Protein (PAPP)-A2 in Physiology and Disease. Cells 10, 3576. https://doi.org/10.3390/cells10123576

Beck, T., Schweikhart, G., Stolz, E., 1986. Immunohistochemical location of HPL, SP1 and β-HCG in normal placentas of varying gestational age. Arch Gynecol 239, 63–74. https://doi.org/10.1007/bf02133965

Bégay, V., Smink, J., Leutz, A., 2004. Essential Requirement of CCAAT/Enhancer Binding Proteins in Embryogenesis. Mol. Cell. Biol. 24, 9744–9751. https://doi.org/10.1128/mcb.24.22.9744-9751.2004

Benirschke, K., Burton, G.J., Baergen, R.N., 2012. Pathology of the Human Placenta 761–880. https://doi.org/10.1007/978-3-642-23941-0_25

Bergen, V., Lange, M., Peidli, S., Wolf, F.A., Theis, F.J., 2020. Generalizing RNA velocity to transient cell states through dynamical modeling. Nat. Biotechnol. 38, 1408–1414. https://doi.org/10.1038/s41587-020-0591-3

Boyd, J.D., Hamilton, W.J., 1970. The Human Placenta. https://doi.org/10.1007/978-1-349-02807-8

Burgos, M.H., Rodríguez, E.M., 1966. Specialized zones in the trophoblast of the human term placenta. Am J Obstet Gynecol 96, 342–356. https://doi.org/10.1016/0002-9378(66)90237-7

Burton, G.J., 1990. On the varied appearances of the human placental villous surface visualised by scanning electron microscopy. Scanning Microscopy 4, 501–7.

Burton, G.J., Jauniaux, E., 1995. Sonographic, stereological and Doppler flow velocimetric assessments of placental maturity. Bjog Int J Obstetrics Gynaecol 102, 818–825. https://doi.org/10.1111/j.1471-0528.1995.tb10849.x

Butler, A., Hoffman, P., Smibert, P., Papalexi, E., Satija, R., 2018. Integrating single-cell transcriptomic data across different conditions, technologies, and species. Nat. Biotechnol. 36, 411–420. https://doi.org/10.1038/nbt.4096

Cain, S.A., Mularczyk, E.J., Singh, M., Massam-Wu, T., Kielty, C.M., 2016. ADAMTS-10 and -6 differentially regulate cell-cell junctions and focal adhesions. Sci. Rep. 6, 35956. https://doi.org/10.1038/srep35956

Cain, S.A., Woods, S., Singh, M., Kimber, S.J., Baldock, C., 2022. ADAMTS6 cleaves the large latent TGFβ complex and increases the mechanotension of cells to activate TGFβ. Matrix Biol. 114, 18–34. https://doi.org/10.1016/j.matbio.2022.11.001

Chen, Y., Siriwardena, D., Penfold, C., Pavlinek, A., Boroviak, T.E., 2022. An integrated atlas of human placental development delineates essential regulators of trophoblast stem cells. Dev. (Camb., Engl.) 149, dev200171. https://doi.org/10.1242/dev.200171

Ching, Y.-P., Wong, C.-M., Chan, S.-F., Leung, T.H.-Y., Ng, D.C.-H., Jin, D.-Y., Ng, I.O., 2003. Deleted in Liver Cancer (DLC) 2 Encodes a RhoGAP Protein with Growth Suppressor Function and Is Underexpressed in Hepatocellular Carcinoma*. J. Biol. Chem. 278, 10824–10830. https://doi.org/10.1074/jbc.m208310200

Clark, D., Smith, S., Licence, D., Evans, A., Charnock-Jones, D., 1998. Comparison of expression patterns for placenta growth factor, vascular endothelial growth factor (VEGF), VEGF-B and VEGF-C in the human placenta throughout gestation. J Endocrinol 159, 459–467. https://doi.org/10.1677/joe.0.1590459

Costa, M.A., 2016. The endocrine function of human placenta: an overview. Reprod Biomed Online 32, 14–43. https://doi.org/10.1016/j.rbmo.2015.10.005

Derisoud, E., Jiang, H., Zhao, A., Chavatte-Palmer, P., Deng, Q., 2024. Revealing the molecular landscape of human placenta: a systematic review and meta-analysis of single-cell RNA sequencing studies. Hum. Reprod. Updat. dmae006. https://doi.org/10.1093/humupd/dmae006

Foxler, D.E., Bridge, K.S., Foster, J.G., Grevitt, P., Curry, S., Shah, K.M., Davidson, K.M., Nagano, A., Gadaleta, E., Rhys, H.I., Kennedy, P.T., Hermida, M.A., Chang, T., Shaw, P.E., Reynolds, L.E., McKay, T.R., Wang, H., Ribeiro, P.S., Plevin, M.J., Lagos, D., Lemoine, N.R., Rajan, P., Graham, T.A., Chelala, C., Hodivala-Dilke, K.M., Spendlove, I., Sharp, T.V., 2018. A HIF–LIMD1 negative feedback mechanism mitigates the pro-tumorigenic effects of hypoxia. EMBO Mol. Med. 10, e8304. https://doi.org/10.15252/emmm.201708304

Haeussner, E., Buehlmeyer, A., Schmitz, C., Koch, F.E. von, Frank, H.-G., 2014. Novel 3D Microscopic Analysis of Human Placental Villous Trees Reveals Unexpected Significance of Branching Angles. Sci. Rep. 4, 6192. https://doi.org/10.1038/srep06192

Haider, S., Meinhardt, G., Saleh, L., Kunihs, V., Gamperl, M., Kaindl, U., Ellinger, A., Burkard, T.R., Fiala, C., Pollheimer, J., Mendjan, S., Latos, P.A., Knöfler, M., 2018. Self-Renewing Trophoblast Organoids Recapitulate the Developmental Program of the Early Human Placenta. Stem Cell Rep 11, 537–551. https://doi.org/10.1016/j.stemcr.2018.07.004

Hao, Y., Hao, S., Andersen-Nissen, E., Mauck, W.M., Zheng, S., Butler, A., Lee, M.J., Wilk, A.J., Darby, C., Zager, M., Hoffman, P., Stoeckius, M., Papalexi, E., Mimitou, E.P., Jain, J., Srivastava, A., Stuart, T., Fleming, L.M., Yeung, B., Rogers, A.J., McElrath, J.M., Blish, C.A., Gottardo, R., Smibert, P., Satija, R., 2021. Integrated analysis of multimodal single-cell data. Cell 184, 3573-3587.e29. https://doi.org/10.1016/j.cell.2021.04.048

Hemberger, M., Hanna, C.W., Dean, W., 2020. Mechanisms of early placental development in mouse and humans. Nat. Rev. Genet. 21, 27–43. https://doi.org/10.1038/s41576-019-0169-4

Hempstock, J., Bao, Y.-P., Bar-Issac, M., Segaren, N., Watson, A.L., Charnock-Jones, D.S., Jauniaux, E., Burton, G.J., 2003. Intralobular Differences in Antioxidant Enzyme Expression and Activity Reflect the Pattern of Maternal Arterial Bloodflow Within the Human Placenta. Placenta 24, 517–523. https://doi.org/10.1053/plac.2002.0955

Hie, B., Bryson, B., Berger, B., 2018. Efficient integration of heterogeneous single-cell transcriptomes using Scanorama. Nat. Biotechnol. 37, 685–691. https://doi.org/10.1038/s41587-019-0113-3

Hie, B., Cho, H., DeMeo, B., Bryson, B., Berger, B., 2019. Geometric Sketching Compactly Summarizes the Single-Cell Transcriptomic Landscape. Cell Syst. 8, 483-493.e7. https://doi.org/10.1016/j.cels.2019.05.003

Jauniaux, E., Hempstock, J., Greenwold, N., Burton, G.J., 2003. Trophoblastic Oxidative Stress in Relation to Temporal and Regional Differences in Maternal Placental Blood Flow in Normal and Abnormal Early Pregnancies. Am J Pathology 162, 115–125. https://doi.org/10.1016/s0002-9440(10)63803-5

Khaliq, A., Li, X.F., Shams, M., Sisi, P., Acevedo, C.A., Whittle, M.J., Weigh, H., Ahmed, A., 2009. Localisation of Placenta Growth Factor (PlGF) in Human Term Placenta. Growth Factors 13, 243–250. https://doi.org/10.3109/08977199609003225

Kim, M., Franke, V., Brandt, B., Lowenstein, E.D., Schöwel, V., Spuler, S., Akalin, A., Birchmeier, C., 2020. Single-nucleus transcriptomics reveals functional compartmentalization in syncytial skeletal muscle cells. Nat Commun 11, 6375. https://doi.org/10.1038/s41467-020-20064-9

Kumar, P., Magon, N., 2012. Hormones in pregnancy. Niger. Méd. J. : J. Niger. Méd. Assoc. 53, 179–183. https://doi.org/10.4103/0300-1652.107549

Li, F., Long, Y., Yu, X., Tong, Y., Gong, L., 2022. Different Immunoregulation Roles of Activin A Compared With TGF-β. Front. Immunol. 13, 921366. https://doi.org/10.3389/fimmu.2022.921366

Li, Q., Sharkey, A., Sheridan, M., Magistrati, E., Arutyunyan, A., Huhn, O., Sancho-Serra, C., Anderson, H., McGovern, N., Esposito, L., Fernando, R., Gardner, L., Vento-Tormo, R., Turco, M.Y., Moffett, A., 2024. Human uterine natural killer cells regulate differentiation of extravillous trophoblast early in pregnancy. Cell Stem Cell 31, 181-195.e9. https://doi.org/10.1016/j.stem.2023.12.013

Li, X., Li, Z.-H., Wang, Y.-X., Liu, T.-H., 2023. A comprehensive review of human trophoblast fusion models: recent developments and challenges. Cell Death Discov. 9, 372. https://doi.org/10.1038/s41420-023-01670-0

Li, Y., Moretto-Zita, M., Leon-Garcia, S., Parast, M.M., 2014. p63 Inhibits Extravillous Trophoblast Migration and Maintains Cells in a Cytotrophoblast Stem Cell-Like State. Am. J. Pathol. 184, 3332–3343. https://doi.org/10.1016/j.ajpath.2014.08.006

Liu, Y., Fan, X., Wang, R., Lu, X., Dang, Y.-L., Wang, Huiying, Lin, H.-Y., Zhu, C., Ge, H., Cross, J.C., Wang, Hongmei, 2018. Single-cell RNA-seq reveals the diversity of trophoblast subtypes and patterns of differentiation in the human placenta. Cell Res 28, 819–832. https://doi.org/10.1038/s41422-018-0066-y

Love, M.I., Huber, W., Anders, S., 2014. Moderated estimation of fold change and dispersion for RNA-seq data with DESeq2. Genome Biol. 15, 550. https://doi.org/10.1186/s13059-014-0550-8

Manno, G.L., Soldatov, R., Zeisel, A., Braun, E., Hochgerner, H., Petukhov, V., Lidschreiber, K., Kastriti, M.E., Lönnerberg, P., Furlan, A., Fan, J., Borm, L.E., Liu, Z., Bruggen, D. van, Guo, J., He, X., Barker, R., Sundström, E., Castelo-Branco, G., Cramer, P., Adameyko, I., Linnarsson, S., Kharchenko, P.V., 2018. RNA velocity of single cells. Nature 560, 494–498. https://doi.org/10.1038/s41586-018-0414-6

Marsh, B., Zhou, Y., Kapidzic, M., Fisher, S., Blelloch, R., 2022. Regionally distinct trophoblast regulate barrier function and invasion in the human placenta. eLife 11, e78829. https://doi.org/10.7554/elife.78829

Mayhew, T.M., 2014. Turnover of human villous trophoblast in normal pregnancy: What do we know and what do we need to know? Placenta 35, 229–240. https://doi.org/10.1016/j.placenta.2014.01.011

Mayhew, T.M., Simpson, R.A., 1994. Quantitative evidence for the spatial dispersal of trophoblast nuclei in human placental villi during gestation. Placenta 15, 837–44. https://doi.org/10.1016/s0143-4004(05)80185-7

Megli, C.J., Coyne, C.B., 2021. Infections at the maternal–fetal interface: an overview of pathogenesis and defence. Nat Rev Microbiol 1–16. https://doi.org/10.1038/s41579-021-00610-y

Mizutani, T., Orisaka, M., Miyazaki, Y., Morichika, R., Uesaka, M., Miyamoto, K., Yoshida, Y., 2022. Inhibition of YAP/TAZ-TEAD activity induces cytotrophoblast differentiation into syncytiotrophoblast in human trophoblast. Mol. Hum. Reprod. 28, gaac032. https://doi.org/10.1093/molehr/gaac032

Moore, T., Williams, J.M., Becerra-Rodriguez, M.A., Dunne, M., Kammerer, R., Dveksler, G., 2021. Pregnancy-specific glycoproteins: evolution, expression, functions and disease associations. Reprod. (Camb., Engl.) 163, R11–R23. https://doi.org/10.1530/rep-21-0390

Morrish, D.W., Marusyk, H., 1997. Localization of human chorionic gonadotropin and placental lactogen by immunogold labeling for electron microscopy: Technique and limitations. Microsc Res Techniq 38, 176–187. https://doi.org/10.1002/(sici)1097-0029(19970701/15)38:1/2<176::aid-jemt18>3.0.co;2-m

Mouzon, S.H., 1997. The GLUT3 Glucose Transporter Isoform Is Differentially Expressed within Human Placental Cell Types. J Clin Endocr Metab 82, 2689–2694. https://doi.org/10.1210/jc.82.8.2689

Okae, H., Toh, H., Sato, T., Hiura, H., Takahashi, S., Shirane, K., Kabayama, Y., Suyama, M., Sasaki, H., Arima, T., 2018. Derivation of Human Trophoblast Stem Cells. Cell Stem Cell 22, 50-63.e6. https://doi.org/10.1016/j.stem.2017.11.004

Pique-Regi, R., Romero, R., Tarca, A.L., Sendler, E.D., Xu, Y., Garcia-Flores, V., Leng, Y., Luca, F., Hassan, S.S., Gomez-Lopez, N., 2019. Single cell transcriptional signatures of the human placenta in term and preterm parturition. Elife 8, e52004. https://doi.org/10.7554/elife.52004

Pirity, M.K., Locker, J., Schreiber-Agus, N., 2005. Rybp/DEDAF Is Required for Early Postimplantation and for Central Nervous System Development. Mol. Cell. Biol. 25, 7193–7202. https://doi.org/10.1128/mcb.25.16.7193-7202.2005

Qu, H., Khalil, R.A., 2022. Role of ADAM and ADAMTS disintegrin and metalloproteinases in normal pregnancy and preeclampsia. Biochem. Pharmacol. 206, 115266. https://doi.org/10.1016/j.bcp.2022.115266

Rodriguez, M.A. de la R., Kersten, S., 2020. Regulation of lipid droplet homeostasis by hypoxia inducible lipid droplet associated HILPDA. Biochim. Biophys. Acta (BBA) - Mol. Cell Biol. Lipids 1865, 158738. https://doi.org/10.1016/j.bbalip.2020.158738

Rose, N.R., King, H.W., Blackledge, N.P., Fursova, N.A., Ember, K.J., Fischer, R., Kessler, B.M., Klose, R.J., 2016. RYBP stimulates PRC1 to shape chromatin-based communication between Polycomb repressive complexes. eLife 5, e18591. https://doi.org/10.7554/elife.18591

Rull, K., Laan, M., 2005. Expression of β-subunit of HCG genes during normal and failed pregnancy. Hum. Reprod. 20, 3360–3368. https://doi.org/10.1093/humrep/dei261

SAMAAN, N., YEN, S.C.C., FRIESEN, H., PEARSON, O.H., 1966. Serum Placental Lactogen Levels During Pregnancy and in Trophoblastic Disease. J. Clin. Endocrinol. Metab. 26, 1303–1308. https://doi.org/10.1210/jcem-26-12-1303

Sasagawa, T., Nagamatsu, T., Morita, K., Mimura, N., Iriyama, T., Fujii, T., Shibuya, M., 2018. HIF-2α, but not HIF-1α, mediates hypoxia-induced up-regulation of Flt-1 gene expression in placental trophoblasts. Sci. Rep. 8, 17375. https://doi.org/10.1038/s41598-018-35745-1

Sasagawa, T., Nagamatsu, T., Yanagisawa, M., Fujii, T., Shibuya, M., 2021. Hypoxia-inducible factor-1β is essential for upregulation of the hypoxia-induced FLT1 gene in placental trophoblasts. Mol. Hum. Reprod. 27, gaab065. https://doi.org/10.1093/molehr/gaab065

Satija, R., Farrell, J.A., Gennert, D., Schier, A.F., Regev, A., 2015. Spatial reconstruction of single-cell gene expression data. Nat. Biotechnol. 33, 495–502. https://doi.org/10.1038/nbt.3192

Shannon, M.J., McNeill, G.L., Koksal, B., Baltayeva, J., Wächter, J., Castellana, B., Peñaherrera, M.S., Robinson, W.P., Leung, P.C.K., Beristain, A.G., 2024. Single-cell assessment of primary and stem cell-derived human trophoblast organoids as placenta-modeling platforms. Dev. Cell 59, 776-792.e11. https://doi.org/10.1016/j.devcel.2024.01.023

Sharkey, A.M., Charnock-Jones, D.S., Boocock, C.A., Brown, K.D., Smith, S.K., 1993. Expression of mRNA for vascular endothelial growth factor in human placenta. Reproduction 99, 609–615. https://doi.org/10.1530/jrf.0.0990609

Shibuya, M., 2011. Vascular Endothelial Growth Factor (VEGF) and Its Receptor (VEGFR) Signaling in Angiogenesis. Genes Cancer 2, 1097–1105. https://doi.org/10.1177/1947601911423031

Silva, C.J.S. da, Simón, R., Busturia, A., 2018. Epigenetic and non-epigenetic functions of the RYBP protein in development and disease. Mech. Ageing Dev. 174, 111–120. https://doi.org/10.1016/j.mad.2018.03.011

Simpson, R.A., Mayhew, T.M., Barnes, P.R., 1992. From 13 weeks to term, the trophoblast of human placenta grows by the continuous recruitment of new proliferative units: A study of nuclear number using the disector. Placenta 13, 501–512. https://doi.org/10.1016/0143-4004(92)90055-x

Singh, R., Wu, A.P., Mudide, A., Berger, B., 2024. Causal gene regulatory analysis with RNA velocity reveals an interplay between slow and fast transcription factors. Cell Syst. 15, 462-474.e5. https://doi.org/10.1016/j.cels.2024.04.005

Street, K., Risso, D., Fletcher, R.B., Das, D., Ngai, J., Yosef, N., Purdom, E., Dudoit, S., 2018. Slingshot: cell lineage and pseudotime inference for single-cell transcriptomics. BMC Genom. 19, 477. https://doi.org/10.1186/s12864-018-4772-0

Stuart, T., Butler, A., Hoffman, P., Hafemeister, C., Papalexi, E., Mauck, W.M., Hao, Y., Stoeckius, M., Smibert, P., Satija, R., 2019. Comprehensive Integration of Single-Cell Data. Cell 177, 1888-1902.e21. https://doi.org/10.1016/j.cell.2019.05.031

Suryawanshi, H., Morozov, P., Straus, A., Sahasrabudhe, N., Max, K.E.A., Garzia, A., Kustagi, M., Tuschl, T., Williams, Z., 2018. A single-cell survey of the human first-trimester placenta and decidua. Sci Adv 4, eaau4788. https://doi.org/10.1126/sciadv.aau4788

Tuohey, L., Macintire, K., Ye, L., Palmer, K., Skubisz, M., Tong, S., Kaitu'u-Lino, T.J., 2013. PLAC4 is upregulated in severe early onset preeclampsia and upregulated with syncytialisation but not hypoxia. Placenta 34, 256–260. https://doi.org/10.1016/j.placenta.2012.12.009

Turco, M.Y., Gardner, L., Kay, R.G., Hamilton, R.S., Prater, M., Hollinshead, M., McWhinnie, A., Esposito, L., Fernando, R., Skelton, H., Reimann, F., Gribble, F., Sharkey, A., Marsh, S.G.E., O'Rahilly, S., Hemberger, M., Burton, G.J., Moffett, A., 2019. Trophoblast organoids as a model for maternal-fetal interactions during human placentation. Nature 564, 263–267. https://doi.org/10.1038/s41586-018-0753-3

Turco, M.Y., Moffett, A., 2019. Development of the human placenta. Development 146, dev163428. https://doi.org/10.1242/dev.163428

Vento-Tormo, R., Efremova, M., Botting, R.A., Turco, M.Y., Vento-Tormo, M., Meyer, K.B., Park, J.-E., Stephenson, E., Polański, K., Goncalves, A., Gardner, L., Holmqvist, S., Henriksson, J., Zou, A., Sharkey, A.M., Millar, B., Innes, B., Wood, L., Wilbrey-Clark, A., Payne, R.P., Ivarsson, M.A., Lisgo, S., Filby, A., Rowitch, D.H., Bulmer, J.N., Wright, G.J., Stubbington, M.J.T., Haniffa, M., Moffett, A., Teichmann, S.A., 2018. Single-cell reconstruction of the early maternal–fetal interface in humans. Nature 563, 347–353. https://doi.org/10.1038/s41586-018-0698-6

Wang, M., Liu, Y., Sun, R., Liu, F., Li, J., Yan, L., Zhang, J., Xie, X., Li, D., Wang, Y., Li, S., Zhu, X., Li, R., Lu, F., Xiao, Z., Wang, H., 2024. Single-nucleus multi-omic profiling of human placental syncytiotrophoblasts identifies cellular trajectories during pregnancy. Nat. Genet. 56, 294–305. https://doi.org/10.1038/s41588-023-01647-w

Wooding, P., Burton, G., 2008. Comparative Placentation, Structures, Functions and Evolution. https://doi.org/10.1007/978-3-540-78797-6

Yang, L., Liang, P., Yang, H., Coyne, C.B., 2023. Trophoblast organoids with physiological polarity model placental structure and function. J. Cell Sci. 137, jcs261528. https://doi.org/10.1242/jcs.261528

Yang, L., Semmes, E.C., Ovies, C., Megli, C., Permar, S., Gilner, J.B., Coyne, C.B., 2022. Innate immune signaling in trophoblast and decidua organoids defines differential antiviral defenses at the maternal-fetal interface. eLife 11, e79794. https://doi.org/10.7554/elife.79794

Zeltz, C., Gullberg, D., 2016. The integrin–collagen connection – a glue for tissue repair? J. Cell Sci. 129, 1284–1284. https://doi.org/10.1242/jcs.188672

Zhu, Y.-N., Pan, F., Gan, X.-W., Liu, Y., Wang, W.-S., Sun, K., 2023. The Role of DNMT1 and C/EBPα in the Regulation of CYP11A1 Expression During Syncytialization of Human Placental Trophoblasts. Endocrinology 165, bqad195. https://doi.org/10.1210/endocr/bqad195